STUDY OF CONFORMATIONAL STABILITY AND CHAIN FLEXIBILITY IN PHOSPHORUS BASED INORGANIC POLYMERS USING DENSITY FUNCTIONAL THEORY METHOD

AMRUTHAVALLI RAJA

STUDY OF CONFORMATIONAL STABILITY AND CHAIN FLEXIBILITY IN PHOSPHORUS BASED INORGANIC POLYMERS USING DENSITY FUNCTIONAL THEORY METHOD

By

©Amruthavalli Raja

M. Sc., S.V. University, India

A THESIS SUBMITTED TO THE SCHOOL OF GRADUATE STUDIES IN PARTIAL FULFILLMENT OF THE REQUIREMENTS FOR THE DEGREE OF MASTERS OF SCIENCE

DEPARTMENT OF PHYSICS

MEMORIAL UNIVERSITY OF NEWFOUNDLAND

NOVEMBER, 1994

ST. JOHN'S NEWFOUNDLAND

ISBN 0-612-01907-1

Table of Contents

List of Tables

List of Figures

Abstract

The structure and conformational stability of poly(thionylphosphazenes) and classical poly(phosphazenes) is investigated by modeling single polymer chains with small mimics. The model compounds are composed of repeat units of the corresponding poly(thionylphosphazenes) and classical poly(phosphazenes). Two of the model compounds of poly(thionylphosphazenes) have hydrogens and two have chlorines as substituents on phosphorus atoms. All model compounds of classical poly(phosphazenes) have only chlorine substituents on phosphorus atoms. In poly(thionylphosphazenes) the substituents on sulfur may be either fluorine or chlorine. Fully geometry optimized structures and energies of the stable conformations involving rotations around P-N bond are obtained using the density functional theory method. The objective of this work is to investigate the flexibility of the chain backbones of the corresponding poly(thionylphosphazenes) and classical poly(phosphazenes). It has been found that for all model compounds the non-planar trans-cis conformations have the lowest total energies. The structural and conformational analyses indicate that the rotation around N–P bond leads to variations in the bond lengths, the SNP, PNP bond angle openings as well as couplings between dihedral angles in different conformations in all model compounds. It was found that the values of the conformational energy differences for poly(thionylphosphazenes) range between 0.6 to 5 kcal/mole and for classical poly(phosphazenes) 0.3 to 1 kcal/mole. The effects of the sulfur and different substituents of sulfur, on conformational stability are discussed. The plots of radial density distribution function, $D(r)=4\pi r^2\rho(r)$ computed from the spherically averaged numerical density are presented and analyzed. Using the spherically averaged total electron densities it is shown that the charge along the backbones of

the model compounds is partially delocalized and accumulates primarily on the nitrogen atoms. The conformational analysis results will be correlated with the experimentally obtained glass transition temperatures.

Chapter 1

Introduction

Polymers with backbones consisting entirely of inorganic elements possess a wide range of unusual properties and potential applications [1]. In this work we are interested in investigating the structure, the conformational stability and the electron charge distribution along the backbone of inorganic polymers, poly(thionylphosphazenes) (PTPs) and classical poly(phosphazenes) (CPP) using a quantum mechanical method.

The general formulas for the PTPs and CPPs polymer repeat units are shown in figures 1.1 and 1.2 where R^1 and R^2 are side groups that may consist of single atoms or groups of atoms [2, 3, 4].

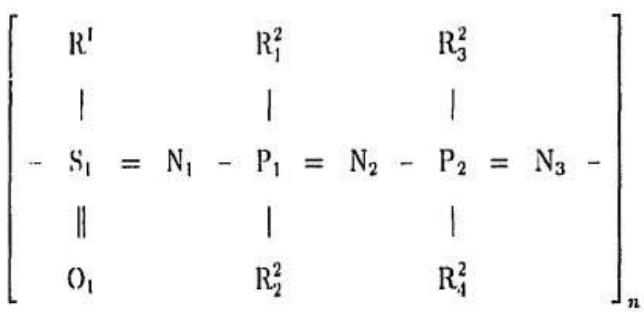

Figure 1.1: The monomer unit of PTP chain.

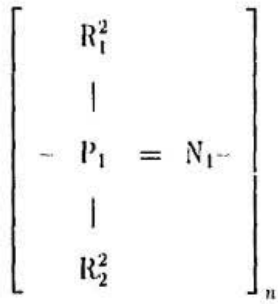

Figure 1.2: The monomer unit of CPP chain.

At the turn of the 20^{th} century, H.N. Stokes, [5, 6, 7] an American chemist, first reported that chlorophosphazenes, when heated, were transformed into an elastomeric material known as 'inorganic rubber', and he suggested a cyclic structure for chlorophosphazenes. It was not known that inorganic rubber was a high polymer with thousands of repeating units linked end to end. During the next 40 years this material was ignored by the mainstream scientists of the day, because of the insolubility of the polymer in all known solvents and its hydrolytic instability in the atmosphere. X-ray diffraction experiments by Meyer, Lotmar, and Pankow [8] in 1936 strongly suggested that this material contained linear high polymeric chain $(NP(Cl_2))_n$. Intensive research in this area began only after mid-1960s with publications of three papers by Allcock, Kugel, and Valan [9, 10, 11]. The hydrolytic sensitivity implies a high reactivity of the P Cl bonds, which might be utilized as a principal advantage in the design of new materials. Replacement of the chlorine atoms by hydrolytically stable organic groups, provides access to a very broad range of stable organic derivative polymers. A linear poly(dichlorophosphazene) polymer is prepared by the ring opening polymerization

of hexachlorocyclo(triphosphazene), $(NP(Cl_2))_3$. When dissolved in a suitable solvent, *poly(dichlorophosphazene)* was found to behave as a remarkable macromolecular reactant. The total replacement of the chlorine atoms by the organic units is possible. Thus, the most important feature of poly(phosphazene) chemistry is that this synthesis allows for a large variety of side groups to be attached to the backbone which in turn produces materials with a broad range of properties [10].

Long-chain polymers based on a skeleton of alternating phosphorus and nitrogen atoms are the 'parent' systems for other macromolecules that contain phosphorus, nitrogen, and some other elements in the skeletal system. One example of this type of system is PTP which contain sulfur, nitrogen, and phosphorus in the backbone. The first, well-characterized PTPs, were reported in 1990 [12]. Typically PTPs are synthesized in the thermal ring–opening polymerization in which cyclic thionylphosphazenes $[(NSOR^1)(NP(Cl_2))]$ (R^1=Cl or F) open to produce a hydrolytically sensitive glassy materials [2, 3, 4].

Even though the phosphorus based polymers are at a very early stage of development, unusual and unique features in the chemistry and material properties are already emerging [4]. They have some of the lowest glass transition temperatures (T_gs) known in polymer chemistry [1]. These unusual properties of a polymer depend very much on the underlying molecular structure, nature of the skeleton, and the type of side groups attached to it [2]. For example $(NP(Cl_2))_n$ has a T_g of −63 °C, $[(NSOR^1)(NP(Cl_2))]$ with R^1=Cl has a T_g of −46 °C and with R^1=F has a T_g of −56 °C. This example illustrates the sensitivity of T_g to substituents and to the presence of a N=S(O)X moiety in the place of a $N{=}PX_2$ (where X=Cl) in chlorine substituted CPPs and PTPs.

The phenomena of glass transition is not very well understood [13], however it is believed that a close connection exists between the skeletal flexibility of the polymer and the glass transition temperature T_g. Below the glass transition temperature, the

polymer is a glass, and the backbone bonds have insufficient thermal energy to undergo significant torsional motions. As the temperature is raised above the T_g, an onset of torsional motion occurs, such that individual molecules can now twist and yield to stress and strain. In this state the polymer is a quasi-liquid. Thus, a polymer with a high T_g is believed to have a backbone that offers more resistance to bond torsion than a polymer with low T_g.

The practical uses of various polymers depend greatly on their T_g value. For example, polystyrene with a T_g of 100°C is applicable for use as a hard glassy material. Ethylene propylene copolymer with a T_g of about −60°C is used as a rubber. The main structural factors resulting in an increase of T_g are related to the increased strength of intermolecular forces and the increased difficulty of internal rotations in single polymer chains. For instance, polystyrene has a T_g of 100°C and poly(acenaphthalene) has a T_g of 285°C. The latter exhibits a much higher hindrance to rotation than does polystyrene.

In summary, it is believed that low glass transition temperature is indicative of a high torsional mobility of the single polymer chain [13]. High chain flexibility can be understood either in a static or in a dynamic sense [14]. The important physical quantity in the determination of static flexibility of the chain is its persistence length. At a given temperature T, the persistence length of the chain is a function of conformational energy differences (the larger the energy differences, the larger the persistence length) [14]. The ratio between the persistence length and the total length of the chain determines the chain flexibility (the smaller the ratio, the greater the static chain flexibility). The dynamic flexibility is a function of the interconversion time interval between the minima. At a given temperature this time interval depends mainly on the height of the energy barriers and the breadth of the minimum energy wells (the heigher the rotational energy barriers the longer the interconversion time interval). Hence, the chain flexibility is mainly a function of three factors:

(i) The magnitude of the conformational energy differences between the local minima and the global minimum energies;

(ii) The breadth of the minimum energy wells and;

(iii) The height of the energy barriers between the principal wells.

In this thesis, only the conformational energy differences will be computed.

The main motivation behind this work is to determine if the changes in T_g (due to the replacement of chlorine by fluorine on sulfur in PTPs and $P(Cl_2)$ by S(OCl) in CPP backbone) can be explained in terms of the corresponding enhancements in the chain flexibilities. From an experimental point of view, PTPs and CPPs form amorphous solids [12] and thus conventional scattering techniques can not be directly applied to extract structures and energies of these systems. From a computational point of view, it is very difficult to determine the molecular structure of these polymers because of their large size. We investigated the structure and the torsional stability of PTPs and CPPs by modeling single polymer chains with small segments of the chains. Small molecules provide critical data about bond lengths, bond angles and torsional angles that could not be obtained directly. The model compounds are composed of repeat units of PTPs and CPPs with methyl end groups (see figures 1.3, 1.4).

We use density functional theory (DFT) method which has been employed successfully in predicting the geometries for a number of molecular systems. We employ a molecular DFT [15, 16] program called *deMon* [17] to perform the complete geometry optimizations. This approach was chosen because it is more computationally expedient than the usual molecular orbital (MO) methods for the large molecular systems that we are considering. This work also serves as a test of using this approach for the inorganic molecules with much larger substituents on phosphorus atoms at a later stage of the investigation. The study of a PTP or CPP polymer molecule with degrees of polymerization typical for materials used in practical applications at theoretical level is not feasible. However,

density functional studies of model compounds or 'mimics' can provide useful information regarding the micro structure of the mimicked macromolecule.

The model compounds, used in this study are composed of a repeat unit of PTPs and CPPs with methyl end groups (see figures 1.3, 1.4).

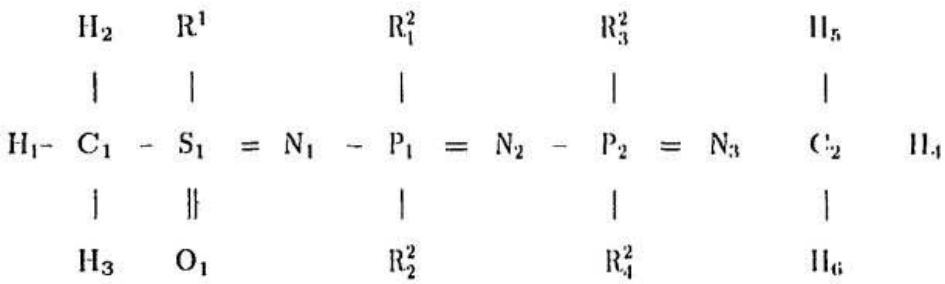

Figure 1.3: The structure of the PTP model compounds.

Two of the model compounds of PTPs have hydrogens as R^2 substituents with R^1 being either fluorine or chlorine. The remaining two model compounds have chlorines as R^2 side groups again with R^1 being either fluorine or chlorine.

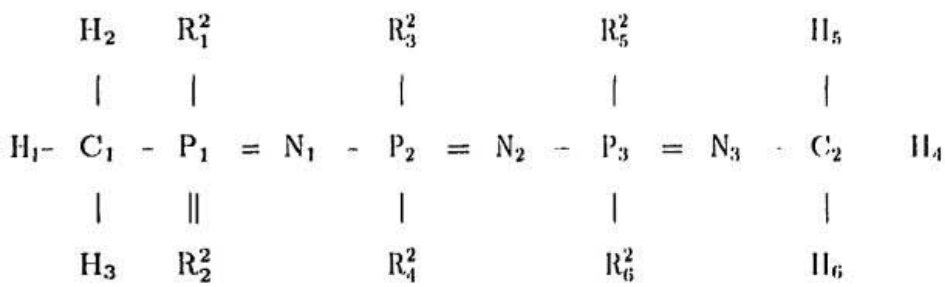

Figure 1.4: The structure of the CPP model compounds.

The model compounds of CPPs have chlorine substituents as R^2 on all phosphorus atoms.

The chain conformation of a macromolecule is determined by the torsional angles assumed by the backbone bonds. In most polymers the torsional angles assumed by the molecule depend on two factors: (1) repulsions or attractions between nearby side groups on the same chain and (2) the forces associated with the packing of many chains into a microcrystalline domain. Because, we are investigating the conformational stability of a model compound, the second factor will not be discussed in this work. In poly(phosphazenes), the conformational energy differences are expected to be smaller than in other classes of macromolecules, since the side groups are attached to every other skeletal atom, rather than to every atom in the chain, thus reducing the interactions between side groups and lowering the energy.

It is hoped that the conformational analysis will lead to resolution of some of the assumptions that are currently being held regarding the chain flexibility in these inorganic compounds. For example, earlier molecular mechanics study [18] in the poly(dihalophosphazenes (also modeled with small chain segments) indicated that they are characterized by very low barriers due to rotation (of the order of 1 kcal/mole) and correspondingly small conformational energy differences (typically less than 1 kcal/mole). This analysis [18] suggests that the conformational energy profiles for these system would be rather flat with energy differences less than 1 kcal/mole. In addition, the authors [18] observed that an approximate correspondence existed between the T_gs of the fluoro, chloro, and bromo derivatives (−95 °C, −63 °C, and −15 °C respectively) and the small increases in barrier heights (and we should add the small increases in the energies of the local minima relative to the lowest minimum). One of the aims of this study is to determine if similar findings also apply to PTP and CPP models whose energies are computed with a quantum mechanical method.

The construction of the complete multidimensional conformational potential energy

surfaces (CPES) at an ab initio level for many-atom systems is currently a computationally prohibitive task. The most important features of the CPES are the stationary points (minima, saddle points and higher order critical points). The pattern that displays only the stationary points of the CPES is referred to as the topological representation of the multidimensional CPES [19, 20]. Frequently, a qualitative topological representation of CPES is used to determine the approximate location of the critical points [21]. This is especially true for organic molecules since in most organic molecules the topology of the computed CPES is similar to that of CPES predicted by the qualitative multidimensional conformational analysis. However, in contrast to the organic molecules (which often behave in this "ideal" manner) it is difficult to construct even a qualitative CPES for inorganic molecules since bonding in these compounds is still not very well understood. Another way of initially estimating the location of the minima with the ab initio methods is to perform rigid rotor calculations (bond lengths and bond angles are held constant as one dihedral angle is changed [19, 20]). In this work, we use two ways of determining the approximate location of the minima in our model compounds: (1) we use the results of rigid-rotor calculations as a guide for their possible locations [22] and (2) we have studied the locations of the minima in simpler systems (such as the hydrogen substituted compounds) and use these findings as an indication of the locations of the minima in model compounds with larger substituents. We focus on finding the minima in the torsion around the N_1–P_1 bond (for PTPs) and N_1-P_2 bond (for CPPs) (see figures 3.1-3.4, 4.1).

The calculations were carried out on a SGI workstations at the Department of Physics, on DEC Alpha workstations available at the Computing and Communication Department at the Memorial University of Newfoundland, and on the Fujitsu Supercomputer at the High Performance Computing Center in Calgary, Alberta. The software packages BIOSYM [23], and MATLAB were used to generate the figures.

In chapter 2 we discuss the theory of density functional formalism and its implementation in *deMon* program. Chapters 3 and 4 we present the results and discussion of our investigations. In chapter 5, the charge density distribution along the backbone of the model compound is discussed. In chapter 6 we correlate the glass transition temperatures with the conformational analysis. In chapter 7 we summarize the results of our calculations and discuss future work.

Chapter 2

Theoretical/Computational Approach

2.1 Density Functional Theory - Basic Formalism

DFT is indispensable in the calculations of electronic structure of large molecules and solids [24, 25, 26, 27]. Over the last three decades, DFT has evolved as a conceptually and practically useful method for studying the electronic properties of many electron systems. In this theory, the many-body problem is reduced to a single electron problem in an effective potential.

We briefly list the important developments that led to the birth of the DFT. Around 1927 - 28, Hartree [28], formulated a mean-field like theory, where each electron is assumed to move in an average classical electrostatic field of all other electrons and the nuclei. Thomas and Fermi [29, 30], related the local electron density, $\rho(\mathbf{r})$, to the total average potential, $V(\mathbf{r})$, experienced by the electron. The later inclusions by Dirac (1930), of a local density functional for the electron-electron exchange energy and by Wigner (1934), of a local electron-electron correlation energy functional, were further contributions for the DFT development. It was found that the leading term in the exchange operator of the Hartree-Fock (HF) equation was proportional to $\rho^{1/3}$, where ρ was the electron density at a given point in real space.

In 1964 Hohenberg and Kohn (HK) [15] formally introduced DFT, a quantum mechanical formalism for many-electron systems which in principle can be solved exactly. HK theorem legitimizes the use of electron density $\rho(\mathbf{r})$ as the basic variable, and states

that all ground state properties of a system are uniquely determined by its charge density $\rho(\mathbf{r})$. HK introduced two theorems. First theorem establishes that the potential $v(\mathbf{r})$ and the ground state (assumed non-degenerate) wave function Ψ are uniquely determined by the electron density $\rho(\mathbf{r})$. The second theorem states that the energy, $E_v(\rho)$ is a minimum for the true ground state densities (i.e. $\delta E_v(\rho)/\delta\rho(\mathbf{r}) - \mu = 0$ where the Lagrange multiplier, μ, accounts for the constraint $N = \int \rho(\mathbf{r})d\mathbf{r}$, where N is the total number of electrons).

Consider a system of N electrons that are moving under the influence of an external potential $v(\mathbf{r})$ and of their mutual Coulomb repulsion. This system can be described by a unique non-degenerate ground state $|\Psi>$. The Hamiltonian has the form,

$$\hat{H} = \hat{T} + \hat{V} + \hat{U} \tag{2.1}$$

where

$$\hat{T} = \frac{1}{2}\int \nabla\psi^*(\mathbf{r}) \cdot \nabla\psi(\mathbf{r})d\mathbf{r} \tag{2.2}$$

$$\hat{V} = \int v(\mathbf{r})\psi^*(\mathbf{r})\psi(\mathbf{r})d\mathbf{r} \tag{2.3}$$

$$\hat{U} = \frac{1}{2}\int \frac{1}{|\mathbf{r}-\mathbf{r}'|}\psi^*(\mathbf{r})\psi^*(\mathbf{r}')\psi(\mathbf{r}')\psi(\mathbf{r})d\mathbf{r}d\mathbf{r}'. \tag{2.4}$$

$\hat{T}$ stands for the kinetic energy operator, $\hat{V}$ represents the interaction of the electrons with the external potential and $\hat{U}$ represents the Coulomb electron-electron interactions. The repulsion energy among nuclear charges is dropped because for a given configuration of atoms, it acts as a constant. The density operator is given by

$$\hat{\rho}(\mathbf{r}) = \psi^*(\mathbf{r})\psi(\mathbf{r}). \tag{2.5}$$

Summation over spin indices is implied.

Recall that we are considering the system of N electrons, moving in an external potential $v(\mathbf{r})$, which have a unique non-degenerate ground state $|\Psi>$; The particle density, $\rho(\mathbf{r})$, is given by the expectation value of the density operator,

$$\rho(\mathbf{r}) \equiv < \Psi | \hat{\rho}(\mathbf{r}) | \Psi > . \tag{2.6}$$

Thus, it follows that Ψ and $\rho(\mathbf{r})$ are unique functionals of $v(\mathbf{r})$. If there are no time-dependent forces in the system, the ground state energy, E, is given by

$$E = < \Psi | \hat{H} | \Psi > . \tag{2.7}$$

HK proved ([15]) that $\rho(\mathbf{r})$ determines $v(\mathbf{r})$, the ground state Ψ and all other electronic properties of the system including the total energy.

Since, $|\Psi>$ is a functional of $\rho(\mathbf{r})$, all many-particle ground state expectation values are functionals of $\rho(\mathbf{r})$. Thus, there exists a universal functional, $F[\rho(\mathbf{r})]$, such that

$$F[\rho(\mathbf{r})] = < \Psi | (\hat{T} + \hat{U}) | \Psi >, \tag{2.8}$$

where $\hat{T}$ and $\hat{U}$ are the kinetic and the Coulombic interaction energy operators. $F[\rho(\mathbf{r})]$ is valid for any number of particles and in any external potential.

For a system of N interacting electrons in a given potential $v(\mathbf{r})$, the ground state energy functional of density $\rho(\mathbf{r})$ is (we are writing E_v for E to show explicit the dependence on v)

$$E_v[\rho(\mathbf{r})] \equiv \int v(\mathbf{r})\rho(\mathbf{r})d\mathbf{r} + F[\rho(\mathbf{r})]. \tag{2.9}$$

The total number of electrons N is given by

$$N = \int \rho(\mathbf{r})d\mathbf{r}. \tag{2.10}$$

It will be shown that $E_v[\rho]$ is a minimum for the "correct" $\rho(\mathbf{r})$ in comparison with values for any other density distributions $\rho'(\mathbf{r})$ with the same total number of particles N.

For non-degenerate $|\Psi>$, it is well known that the conventional Rayleigh-Ritz functional of $|\Psi'>$,

$$\mathcal{E}_v[\Psi'] \equiv <\Psi'|\hat{V}|\Psi'> + <\Psi'|(\hat{T}+\hat{U})|\Psi'> \tag{2.11}$$

has a minimum value for the correct ground state $|\Psi>$ in comparison with any other $|\Psi'>$ with the same number of electrons. Let $|\Psi'>$ be the ground state associated with a different density, $\rho'(\mathbf{r})$, then

$$\begin{aligned} \mathcal{E}_v[\Psi'] &= \int v(\mathbf{r})\rho'(\mathbf{r})d\mathbf{r} + F[\rho'] \\ > \quad \mathcal{E}_v[\Psi] &= \int v(\mathbf{r})\rho(\mathbf{r})d\mathbf{r} + F[\rho]. \end{aligned} \tag{2.12}$$

This establishes the asserted minimum principle for $E_v[\rho]$, and it follows that we can write

$$E_v[\rho] < E_v[\rho']. \tag{2.13}$$

It is clear from the equations (2.8) and (2.9) that this minimum value $E_v[\rho]$, is the correct ground state energy associated with $v(\mathbf{r})$ and N. In other words, $E_v[\rho]$ is minimum for the ground state density, $\rho(\mathbf{r})$. The main problem of DFT is that the functional form of $F[\rho]$ (see equation 2.9) is not known.

It is convenient to separate out the classical Coulomb energy from $F[\rho]$ because of the long range of the Coulomb interactions in the system and write

$$F[\rho] = \frac{1}{2}\int \frac{\rho(\mathbf{r})\rho(\mathbf{r}')}{|\mathbf{r}-\mathbf{r}'|}d\mathbf{r}d\mathbf{r}' + G[\rho] \tag{2.14}$$

where the first term is the classical Coulomb repulsion energy and G[ρ] is a universal functional similar to $F[\rho]$, which is also unknown. With this separation the energy functional, $E_v[\rho]$, becomes

$$E_v[\rho] = \int v(\mathbf{r})\rho(\mathbf{r})d\mathbf{r} + \frac{1}{2}\int \frac{\rho(\mathbf{r})\rho(\mathbf{r}')}{|\mathbf{r}-\mathbf{r}'|}d\mathbf{r}d\mathbf{r}' + G[\rho]. \tag{2.15}$$

The practical implementation of the minimal principle is dependent on the availability of sufficiently accurate approximations for G[ρ].

2.2 Kohn - Sham Equations

One way of implementing DFT formalism is to follow the approach proposed by Kohn and Sham (KS) [16]. This approach (also called the s-system method) involves solving the self-consistent, one-electron equations similar to the Hartree equations. To obtain these equations KS decomposed G[ρ] as follows:

$$G[\rho] = T_s[\rho] + E_{xc}[\rho] \tag{2.16}$$

where $T_s[\rho]$ is the kinetic energy functional for a non-interacting electron gas of density $\rho(\mathbf{r})$ in an external potential $v(\mathbf{r})$ and $E_{xc}[\rho(\mathbf{r})]$ is the exchange-correlation energy functional. $E_{xc}[\rho(\mathbf{r})]$ contains the difference between $T[\rho]$ and $T_s[\rho]$, presumably fairly small, and the nonclassical part of $U[\rho]$. With these quantities E_v can be written as,

$$E_v[\rho] = T_s[\rho] + \int v(\mathbf{r})\rho(\mathbf{r})d\mathbf{r} + \frac{1}{2}\int \frac{\rho(\mathbf{r})\rho(\mathbf{r}')}{|\mathbf{r}-\mathbf{r}'|}d\mathbf{r}d\mathbf{r}' + E_{xc}[\rho(\mathbf{r})]. \tag{2.17}$$

The main thrust of DFT formalism involves the determination of the functional form of $E_{xc}[\rho(\mathbf{r})]$.

The exact form of the exchange-correlation energy functional is not known. Several approximations for $E_{xc}[\rho]$ had been and are still being proposed. DFT theory converges to the exact solution by improving the description of the total exchange correlation energy functional, E_{xc}. The calculations in our work have been performed using the local density approximation (LDA) for the $E_{xc}[\rho]$ [15, 16]. This approximation will be discussed below.

Applying the variational principle to $E_v[\rho]$,

$$\frac{\delta T_s(\rho(\mathbf{r}))}{\delta\rho(\mathbf{r})} + v(\mathbf{r}) + \int \frac{\rho(\mathbf{r}')}{|\mathbf{r}-\mathbf{r}'|}d\mathbf{r}' + \frac{\delta E_{xc}\rho(\mathbf{r})}{\delta\rho(\mathbf{r})} - \mu = 0 \tag{2.18}$$

or

$$\frac{\delta T_s(\rho(\mathbf{r}))}{\delta\rho(\mathbf{r})} + V_c(\mathbf{r}) + v_{xc}(\mathbf{r}) - \mu = 0 \tag{2.19}$$

where $V_c(\mathbf{r})$ is the total classical potential energy

$$V_c(\mathbf{r}) = v(\mathbf{r}) + \int \frac{\rho(\mathbf{r}')}{|\mathbf{r} - \mathbf{r}'|} d\mathbf{r}', \tag{2.20}$$

$v_{xc}(\mathbf{r})$ (exchange-correlation energy potential) is a functional derivative of E_{xc}

$$v_{xc}[\rho(\mathbf{r})] = \frac{\delta E_{xc}}{\delta \rho(\mathbf{r})}, \tag{2.21}$$

and , is the Lagrange multiplier that accounts for the constraints that N is constant (2.10). Equation (2.19) can be rewritten as

$$\frac{\delta T_s(\rho(\mathbf{r}))}{\delta \rho(\mathbf{r})} + v_{eff}(\mathbf{r}) - \mu = 0 \tag{2.22}$$

where

$$v_{eff}(\mathbf{r}) = V_c + v_{xc}(\mathbf{r}) \tag{2.23}$$

$$= v(\mathbf{r}) + \int \frac{\rho(\mathbf{r}')}{|\mathbf{r} - \mathbf{r}'|} d\mathbf{r}' + v_{xc}(\mathbf{r}). \tag{2.24}$$

Equation (2.24) has a similar form to the stationary Schrodinger equation that one would obtain for a system of non-interacting electrons moving in the effective potential, v_{eff}. The effective potential $v_{eff} = V_c(\mathbf{r}) + v_{xc}[\rho(\mathbf{r})]$ acts as an external potential for the non-interacting reference system. In conventional quantum mechanics, for a given v_{eff} the corresponding single particle equations are

$$[-\frac{1}{2}\nabla^2 + v_{eff}(\mathbf{r})]\psi_i(\mathbf{r}) = \varepsilon_i \psi_i(\mathbf{r}) \tag{2.25}$$

with

$$\rho(\mathbf{r}) = \sum_{i=1} n_i |\psi_i(\mathbf{r})|^2 \tag{2.26}$$

where ψ_is are single electron eigenfunctions with eigenvalues ε_i and n_i are the occupation numbers (spin is included in the index i).

Equations (2.25) are called KS one-particle equations. v_{eff} depends on $\rho(\mathbf{r})$ through (2.21); hence (2.24), (2.25) and (2.26) must be solved self-consistently. One begins with a guess for $\rho(\mathbf{r})$, constructs v_{eff} from (2.24) and then finds a new $\rho(\mathbf{r})$ from (2.25) and (2.26).

2.3 The Local Density Approximation

An explicit form for $E_{xc}[\rho]$ is needed to specify the Kohn-Sham equations. The search for an accurate $E_{xc}[\rho]$ has encountered significant difficulties and continues to be the greatest challenge in the DFT. The most often used approximation to the exchange correlation energy is the so-called Local Density Approximation (LDA) proposed by KS [16]. For metallic and strongly delocalized systems with nearly constant electron density, the LDA comes very close to the exact solution whereas this approximation can be expected to be less accurate for systems with strongly varying electron densities.

If the density of the system is slowly varying, then each small part of the electronic system can be thought of as homogeneous, suggesting the following approximation to $E_{xc}[\rho]$.

$$E_{xc}^{LDA}[\rho] = \int d\mathbf{r}\rho(\mathbf{r})\varepsilon_{xc}[\rho]. \tag{2.27}$$

where $\varepsilon_{xc}[\rho]$ is the exchange-correlation energy per electron of a homogeneous electron gas of density ρ.

So, the corresponding exchange-correlation potential becomes,

$$v_{xc}^{LDA}(\mathbf{r}) = \frac{\delta E_{xc}^{LDA}}{\delta\rho(\mathbf{r})} = \frac{\delta\rho(\mathbf{r})\varepsilon_{xc}[\rho(\mathbf{r})]}{\delta\rho(\mathbf{r})} = \varepsilon_{xc}(\rho(\mathbf{r})) + \rho(\mathbf{r})\frac{\delta\varepsilon_{xc}(\rho)}{\delta\rho}. \tag{2.28}$$

In the LDA the KS orbital equations can be written as,

$$[-\frac{1}{2}\nabla^2 + v(\mathbf{r}) + \int \frac{\rho(\mathbf{r}')}{|\mathbf{r}-\mathbf{r}'|}d\mathbf{r}' + v_{xc}^{LDA}(\mathbf{r})]\psi_i = \varepsilon_i\psi_i. \tag{2.29}$$

This equation is solved in self-consistent manner.

The function $\varepsilon_{xc}(\rho)$ can be further divided into exchange and correlation contributions,

$$\varepsilon_{xc}(\rho) = \varepsilon_x(\rho) + \varepsilon_c(\rho). \tag{2.30}$$

The exchange part is given by the Dirac exchange-energy functional,

$$\varepsilon_x(\rho) = -C_x\rho(\mathbf{r})^{\frac{1}{3}}, C_x = \frac{3}{4}(\frac{3}{\pi})^{\frac{1}{3}} \tag{2.31}$$

Accurate values of $\varepsilon_c(\rho)$ are available. Vosko, Wilk, and Nusair (VWN) [31] proposed an analytic form for $\varepsilon_c(\rho)$ by interpolating the quantum Monte Carlo calculation results of Ceperley and Alder [32]. The most commonly used forms are those by Hedin and Lundqvist (1972) [33] and Vosko, Wilk, and Nusair (VWN) [31]. The LDA comes very close to the exact solution for systems with constant electron density. But, this approximation can be expected to be less accurate for systems with strongly varying electron densities.

2.4 Gaussian-Based Density Functional Methodology.

The theoretical investigations for molecular systems usually begin with the HF [19, 20] approximation. In this approximation the molecular orbitals are expanded in terms of the contracted gaussians basis functions centered on the atoms. (For example the programs that employ this method are GAUSSIAN 92, HONDO[19, 20]). HF approximation is also a starting point for more accurate calculations, which include the effect of electron correlation. In this work the energy calculations have been performed with the molecular density functional[15, 16] program called *deMon*[17]. In agreement with the more conventional approach, the program employs a linear combination of gaussian–type orbitals (LCGTO) to create the spatial molecular orbitals which in turn are used to create the total electronic wave functions for the given molecular system. DFT methods have many

advantages over traditional *ab initio* HF self-consistent-field molecular-orbital methods. They are: (1) the DFT allows for the inclusion of the correlation while maintaining the single particle picture of the HF theory; (2) the DFT calculations are not as computationally demanding, as their cost grows nominally as the third power of the number of basis functions, compared to the fourth and higher dependence of traditional methods. (3) the decrease in the computational complexity (mainly due to the simplified treatment of exchange potential in DFT) could in principle allow for the use of larger basis set.

In order to perform geometry optimization we must be able to compute the gradients of the total energy with respect to the nuclear coordinates. Second order derivatives of the total energy (Hessian matrix) are used to determine which points on CPES are minima or transition states. In *deMon*, the analytical expressions for the gradients are computed as discussed in reference [34]. Although, the theory of analytic second derivatives within DFT have been established [35, 36], they have not yet been implemented in *deMon*. At present they are evaluated by the numerical differentiation of the analytical gradients [37, 38, 39, 40, 41]. The stationary points are found using the Broyden-Fletcher-Goldfarb-Shanno (BFGS) (quasi-Newton) algorithm [42]. Full geometry optimization was carried out for all model compounds investigated in this work. The geometries were optimized until the norm of the gradient was less than 0.0008 au.

From the previous section, the total energy functional (equation (2.17)) may be partitioned as

$$E[\rho] = T_s[\rho] + S[\rho] + E_{xc}[\rho] \tag{2.32}$$

where $T_s[\rho]$ is the kinetic energy functional of a system of non-interacting particles, $S[\rho]$ is (middle two terms of the equation (2.17) are combined) the classical electrostatic energy (e-n attraction and e-e repulsion) and $E_{xc}[\rho]$ is the exchange correlation energy functional.

In *deMon* the kinetic energy component and Coulomb components of eqn. (2.32) may be expressed as,

$$T_s = \sum_i^N \left\langle \psi_i(\mathbf{r}) \left| \frac{-\nabla^2}{2} \right| \psi_i(\mathbf{r}) \right\rangle \tag{2.33}$$

$$\begin{aligned} S &= \sum_i^N \left\langle \psi_i(\mathbf{r}) \left| \sum_a^M \frac{-Z_a}{|\mathbf{R}-\mathbf{r}|} \right| \psi_i(\mathbf{r}) \right\rangle + \\ &\frac{1}{2} \sum_i^N \sum_j^N \left[\psi_i(\mathbf{r})\psi_i(\mathbf{r}) \left| \frac{1}{|\mathbf{r}-\mathbf{r}'|} \right| \psi_j(\mathbf{r}')\psi_j(\mathbf{r}') \right] \end{aligned} \tag{2.34}$$

where M is the total numer of nuclei in the system. The charge density, $\rho(\mathbf{r})$ is given as in equation (2.26).

In the gaussian based DFT methodology, (*deMon* program), the spin molecular orbitals (from now on the spin dependence will be shown explicitly), $\{\psi_i^\sigma(\mathbf{r})\}$, ($\sigma = \alpha$ or β), are expanded in terms of linear combination of gaussian-type orbitals (LCGTO).

$$\psi_i^\sigma(\mathbf{r}) = \sum_\mu C_{\mu i}^\sigma \chi_\mu(\mathbf{r}) \tag{2.35}$$

where the set $\{\chi_\mu(\mathbf{r})\}$ are the basis of atom-centered gaussian type orbitals (GTO) and $\{C_{\mu i}^\sigma\}$ are the set of expansion coefficients. We have used double-zeta valence basis set with polarization function [17]. For the elements B to Ne, this basis set is made from nine s-type and five p-type primitive Cartesian Gaussians (Cartesian Gaussians are used since the geometry optimization in *deMon* is done using Cartesian coordinates), augmented by one d-type polarization function [43]. These primitives written as (621/41/1) are contracted to three s-type, and two p-type functions, [3/2/1]. For the elements Al to Ar, the basis set is made from twelve s-type, eight p-type and one d-type primitive Cartesian Gaussians, (6321/521/1) . The corresponding contraction for this basis set is [4/3/1]. The total number of orbital basis functions varied from 182 to 254 depending on the atomic composition of the molecular system studied.

The gaussian bases used in *deMon* are similar to those of used for traditional *ab initio* methods [43]. In terms of these coefficients the total electronic density is given by

$$\rho(\mathbf{r}) = \sum_{i,\sigma} n_i \{ \sum_{\mu=1} \sum_{\lambda=1} C^{\sigma}_{\mu i} C^{\sigma}_{\lambda i} \chi_{\mu}(\mathbf{r}) \chi_{\lambda}(\mathbf{r}) \}. \tag{2.36}$$

In *deMon* (for ease of computing) the charge density, $\rho(\mathbf{r})$, and the exchange correlation potentials, $v^{\sigma}_{xc}(\sigma = \alpha \text{ or } \beta)$, are fitted by an auxiliary basis set (also a LCGTO) [44, 45], i.e.,

$$\tilde{\rho}(\mathbf{r}) = \sum_i a_i f_i(\mathbf{r}) \tag{2.37}$$

$$\tilde{v}^{\sigma}_{xc}(\mathbf{r}) = \sum_i b^{\sigma}_i g_i(\mathbf{r}) \tag{2.38}$$

where $\tilde{\rho}(\mathbf{r})$ and $\tilde{v}^{\sigma}_{xc}(\mathbf{r})$ are the fitted quantities to ρ and v^{σ}_{xc} and $\{f_i(\mathbf{r})\}$ and $\{g_i(\mathbf{r})\}$ are the auxiliary bases and $\{a_i\}$ and $\{b^{\sigma}_i\}$ are the fitting coefficients. These fits reduce integral evaluation from an N^4 process to an N^2M process (where N is the number of GTO's in the orbital basis and M is the total number of GTO's in the auxiliary basis and is typically of comparable size to N).

The two-electron integrals,

$$\left[\chi_{\mu} \chi_{\nu} \left| \frac{1}{r_{12}} \right| f_i \right], \tag{2.39}$$

$$< \chi_{\mu} | g_i | \chi_{\nu} > \tag{2.40}$$

as well as the one electron integrals (which are identical to those in the HF formalism) are evaluated with the efficient formulas of Obara and Saika [46].

The coefficients for the fitting of $\rho(\mathbf{r})$, $\{a_i\}$ are obtained by a least squares fitting procedure which minimizes the error in the Coulomb repulsion energy [45],

$$\left[\rho - \tilde{\rho} \left| \frac{1}{r_{12}} \right| \rho - \tilde{\rho} \right] \tag{2.41}$$

subject to the constraint,

$$< \tilde{\rho} >= N \tag{2.42}$$

which ensures that the fitted charge density is normalized to the total number of electrons, N.

The fitting of ρ is analytical. This is not the case for the fitting of $v^{\sigma}_{xc}(\mathbf{r})$. The coefficients for the fits to the exchange-correlation potentials, $\{b^{\sigma}_{i}\}$, can not be obtained analytically as above for $\{a_i\}$. The fitting coefficients are obtained by minimizing the error in the fitted potentials over the sum of the grid points,

$$\sum_{I}(\tilde{v}^{\sigma}_{xc}(I) - v^{\sigma}_{xc}(I))^2 W(I) W'(I) \tag{2.43}$$

The summation is over a set of points on which the density is synthesized and then the exchange correlation potentials, $v^{\sigma}_{xc}(I)$ calculated. $W(I)$ is the weight attributed to each point I of the grid, is proportional to the volume of space associated with the I^{th} point. $W'(I)$ is an arbitrary weight which may be associated to the I^{th} point. An arbitrary weight is introduced since the purpose of the grid is to perform a fit to the exchange-correlation potentials and not to perform a numerical integration. Dunlap et al [47, 48]. have proposed the arbitrary weighting function,

$$W'(r) = \frac{\rho(\mathbf{r})}{\varepsilon_{xc}(r)} \tag{2.44}$$

where ε_{xc} is the exchange-correlation energy density.

The auxiliary basis sets used in *deMon* are comprised of a set of s type functions and a set of s, p and d type functions constrained to the same exponent. This constraint does not affect the quality of the calculations but speeds up the calculation considerably [49].

The electronic density, $\rho(\mathbf{r})$ is given by

$$\rho(\mathbf{r}) \;=\; \sum_{\sigma}\rho^{\sigma}(\mathbf{r}) = \sum_{i\sigma} n^{\sigma}_{i}|\psi^{\sigma}_{i}(\mathbf{r})|^2 \tag{2.45}$$

$$= \sum_{i\sigma} n_i^\sigma \left[\sum_\nu C_{\nu i}^\sigma \chi_\nu(\mathbf{r}) \sum_\mu C_{\mu i}^\sigma \chi_\mu(\mathbf{r}) \right] \tag{2.46}$$

$$= \sum_{\mu\nu} \left[\sum_{i\sigma} n_i^\sigma C_{\mu i}^\sigma C_{\nu i}^\sigma \right] \chi_\mu(\mathbf{r}) \chi_\nu(\mathbf{r}) \tag{2.47}$$

$$= \sum_{\mu\nu} \left[\sum_i n_i^\alpha C_{\mu i}^\alpha C_{\nu i}^\alpha + \sum_i n_i^\beta C_{\mu i}^\beta C_{\nu i}^\beta \right] \chi_\mu(\mathbf{r}) \chi_\nu(\mathbf{r}) \tag{2.48}$$

$$= \sum_{\mu\nu} P_{\mu\nu}^T \chi_\mu(\mathbf{r}) \chi_\nu(\mathbf{r}) \tag{2.49}$$

where

$$P_{\mu\nu}^T = P_{\mu\nu}^\alpha + P_{\mu\nu}^\beta = \sum_i n_i^\alpha C_{\mu i}^\alpha C_{\nu i}^\alpha + \sum_i n_i^\beta C_{\mu i}^\beta C_{\nu i}^\beta \tag{2.50}$$

$P_{\mu\nu}^T$ is the element of the density matrix and n_i^σ is the occupation number of the orbital $\psi_i^\sigma(\mathbf{r})$.

The electron density $\rho(\mathbf{r})$ is a function of the set of LCGTO coefficients, $\{C_{\mu i}^\sigma\}$. These coefficients are obtained form the Kohn-Sham equations, which are the analog of the Hartree-Fock-Roothaan equations in the traditional *ab initio* theory,

$$\sum_\nu F_{\mu\nu}^\sigma C_{\nu i}^\sigma = \varepsilon_i^\sigma \sum_\nu S_{\mu\nu} C_{\nu i}^\sigma \tag{2.51}$$

where $S_{\mu\nu}$ is an element of the overlap matrix,

$$S_{\mu\nu} = < \mu | \nu >, \tag{2.52}$$

$F_{\mu\nu}^\sigma$ is an element of the Fock-like matrix of spin σ,

$$F_{\mu\nu}^\sigma = h_{\mu\nu} + \left[\chi_\mu \chi_\nu \left| \frac{1}{r_{12}} \right| \tilde{\rho} \right] + \langle \chi_\mu | v_{xc}^\sigma | \chi_\nu \rangle , \tag{2.53}$$

and $\{\varepsilon_i^\sigma\}$ are the orbital energies. In DFT the meaning of ε_i^σ is different from that of traditional *ab initio* methods. Instead of Koopman's theorem [50], we have,

$$\varepsilon_i^\sigma = \frac{\delta E}{\delta n_i^\sigma}. \tag{2.54}$$

The set of equations (2.51) is obtained by minimizing the expression for the total energy with respect to the $C^{\sigma}_{\mu i}$'s, subject to the orthonormalization constraints,

$$\sum_{\mu\nu} C^{\sigma}_{\mu i} S_{\mu\nu} C^{\sigma}_{\nu i} = \delta_{ij}. \tag{2.55}$$

Grid Generation and the Fitting of Exchange-Correlation

One of the most important parts of *deMon* is the algorithm that was chosen to generate the grid on which the exchange and correlation terms are synthesized. Exchange and correlation contributions to energy can not be evaluated analytically, therefore must be calculated numerically on a grid or be fitted to a set of gaussians to minimize the error on the set of points of the grid to then allow the analytical evaluation of exchange and correlation integrals [44, 45].

Many types of grids for fitting the exchange–correlation potentials have been proposed. Most grids for molecular calculations are based on superimposed atom-centred grids. For these atom-centred grids, many radial grids have been proposed [51, 48, 52]. Becke's molecular grid [52] was chosen for the radial grid used in *deMon*. In Becke's approach the molecular integration is decomposed into a sum of one-center, atom-like integrations. Becke's algorithm uses the Gauss-Legendre quadrature scheme instead of Gauss-Chebyshev. In addition to the radial grid, a suitable angular grid is needed. Angular grids designed for accurate integration on the unit sphere by Lebedev are employed in *deMon* [53, 54]. *deMon* offers three angular grids of different quality (with 50, 110, and 194 angular points), which integrate exactly all spherical harmonics of order 11, 17, and 23 or less.

Becke's approach allows for overlap between the discrete regions, each region associated with an atom. To avoid the double counting in the overlap regions, a relative weight, $W''(I)$ is assigned to each grid point. The sum of the relative weights is normalized for each **r** point in space.

It was realized that XC fitting bases are inadequate when calculating the XC contribution to the energy gradient. So, the XC term of the energy gradient expression had to be calculated numerically over an augmented set of grid points, whereas the XC contributions to the Fock matrices, in the SCF procedure, are calculated analytically following the numerical LSF procedure using a modest XC auxiliary basis and a much smaller subset of grid points [45]. This "analytical energy - numerical gradient" procedure seems to be necessary, if both the CPU savings in the SCF step and an accurate energy gradient are required.

Chapter 3

Poly(thionylphosphazenes)

In this section we will present the results of the DFT calculations for the inorganic polymers, poly(thionylphosphazenes) [55]. We label the model compounds in the following way:

model 1 with R^1= F, R^2=H;
model 2 with R^1= Cl, R^2=H;
model 3 with R^1= F, R^2=Cl;
model 4 with R^1= Cl, R^2=Cl.

The rotation around N_1–P_1 bond is indicated as ϕ in figures 3.1–3.4. The completely optimized geometrical parameters (that is bond lengths, bond angles and dihedral angles), the energies and the corresponding energy differences between the global and the local minima conformations are given in tables (3.1–3.16). The torsional angles ϕ's are given as N_2P_1–N_1S_1 dihedral angles. 0_0 denotes the global minimum structure and 0_n (n=1,2..) denote the local minima structures. The subscript n corresponds to energy values according to the following scheme: the smaller the value, the lower the energy. The geometry optimized non–planar, trans–cis (by convention, the dihedral angles 0° and 180° are used to define trans–cis conformation), global minimum structures for the model 1–4 compounds are displayed in the figures 3.1–3.4 respectively.

To see the complete effect of S=O group on the structure and to minimize the effect of end groups on the backbone structure, we investigated the global minimum structures

of two other model compounds (5 and 6) with one more P-N bond near the end group along the backbone. The model compounds are labeled as:

model 5 with R^1= F,R^2=Cl;

model 6 with R^1= Cl,R^2=Cl.

The geometry optimized global minimum structures for the model 5 6 compounds are displayed in the figures 3.5 and 3.6 respectively. Completely optimized geometrical parameters are given in tables (3.17–3.18)

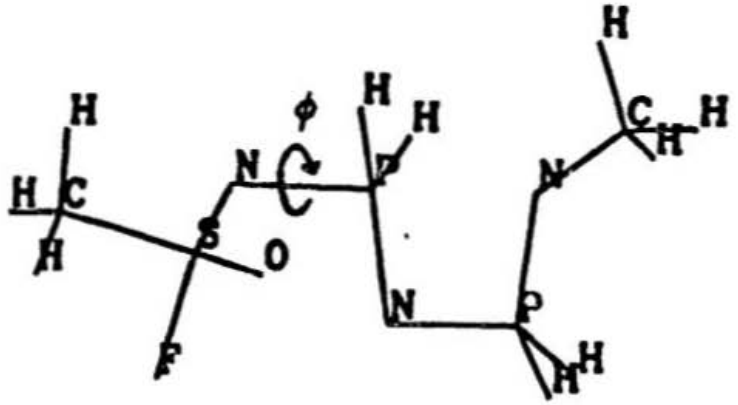

Figure 3.1

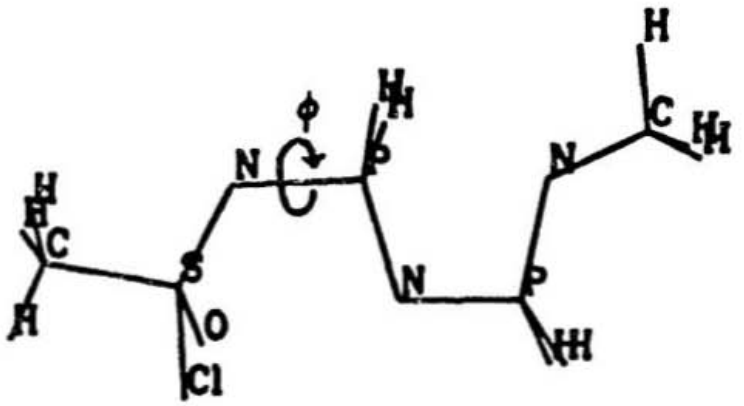

Figure 3.2

Figure 3.1: Stick figure of model 1 compound (R^1=F and R^2_n (n=1-4) =H) with the plane formed by P-N-P atoms parallel to the paper.

Figure 3.2: Stick figure of model 2 compound (R^1=Cl and R^2_n (n=1-4) =H) with the plane formed by P-N-P atoms parallel to the paper. The geometries plotted correspond to the global minimum parameters given in tables (3.1—3.8).

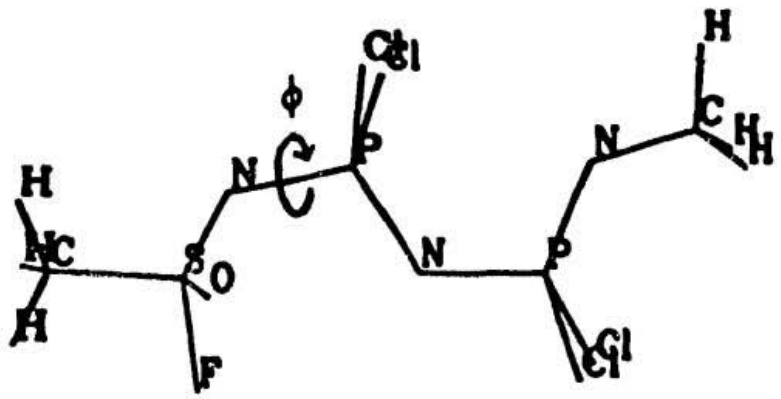

Figure 3.3

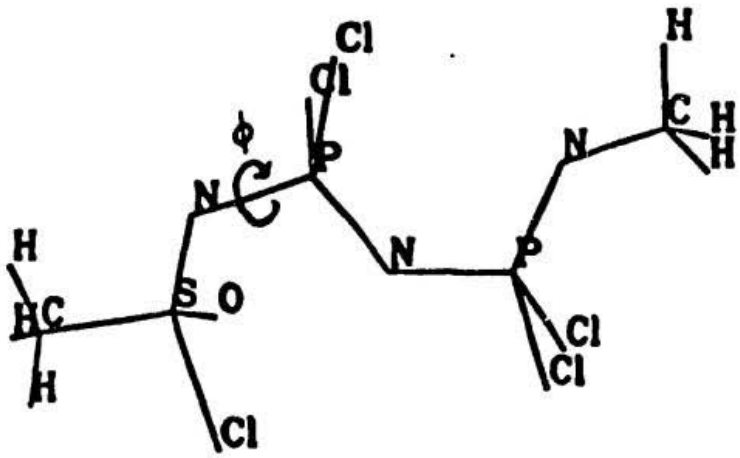

Figure 3.4

Figure 3.3: Stick figure of model 3 compound (R^1=F and R^2 R^2_n (n=1-4) =Cl) with the plane formed by P-N-P atoms parallel to the paper.

Figure 3.4: Stick figure of model 4 compound (R^1=Cl and R^2_n (n=1-4) =Cl) with the plane formed by P-N-P atoms parallel to the paper. The geometries plotted correspond to the global minimum parameters given in tables (3.9—3.16).

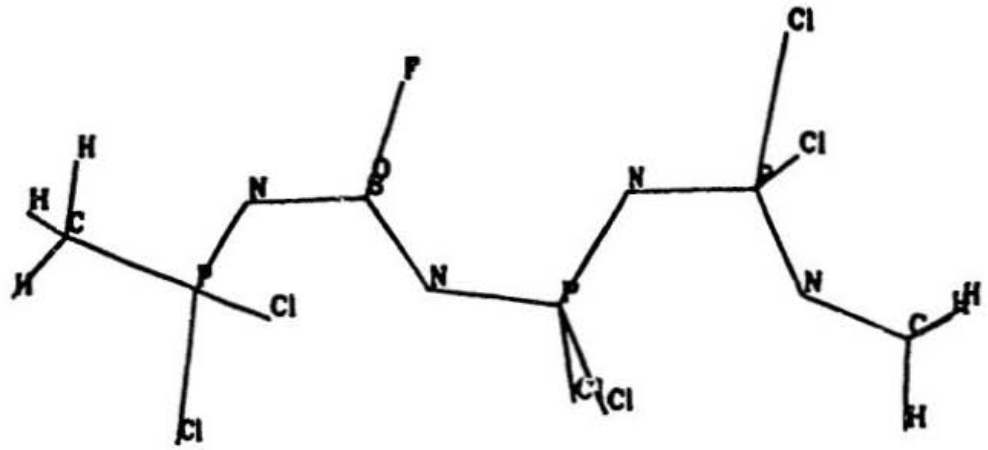

Figure 3.5

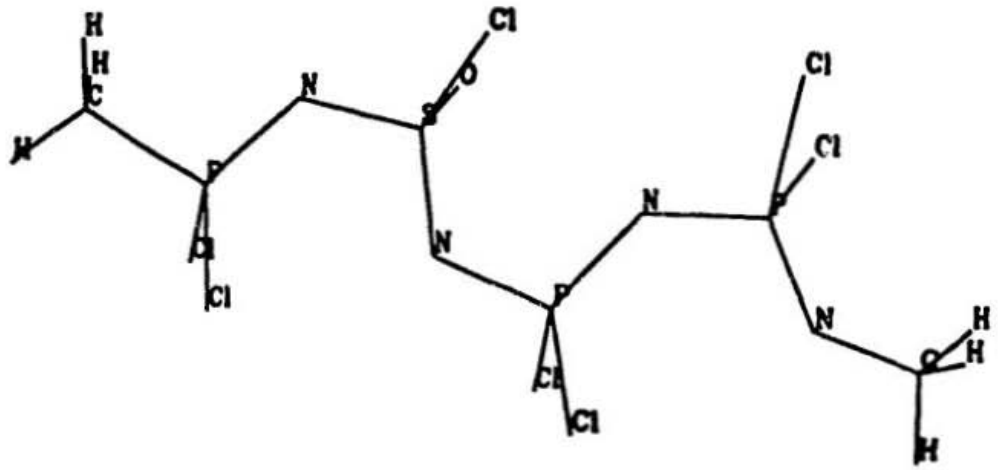

Figure 3.6

Figure 3.5: Stick figure of model 5 compound (R^1=F and R^2 R^2_n (n=1-4) =Cl) with the plane formed by P-N-P atoms parallel to the paper.

Figure 3.6: Stick figure of model 6 compound (R^1=Cl and R^2_n (n=1-4) =Cl) with the plane formed by P-N-P atoms parallel to the paper. The geometries plotted correspond to the global minimum parameters given in tables (3.17—3.18).

3.1 Structural Analysis

(i) Hydrogen Substituted Model Compounds

Hydrogen substituted PTPs have not been synthesized. However, we have chosen to begin our theoretical investigation with hydrogen substituents since they are the simplest and the smallest substituents that can be considered which from the computational point of view is an advantage. In particular, we use the conformational analysis performed for the hydrogen substituted compound as a guide in locating the local minima in compounds with larger substituents on the phosphorus atoms. Moreover the hydrogenated compounds highlight the structural and energetic differences between compounds due to the presence of F or Cl on the sulfur since the complicated interactions between F or Cl with other chlorines on the phosphorus atoms do not arise in this case.

For the model 1 compound (with R^1=F) we have found four local minima in addition to the global one. In agreement with our recent studies [56, 57, 58] we found bond length alternation along backbones of the molecular models for all conformations (see table (3.1)). In all cases the "single" and "double" bonds of the N P type are longest near sulfur. It is suspected that pattern is in part due to the end effects. The bond N_1 P_1 exhibits largest variations in length due to rotation around N_1-P_1 bond. For example the difference of 0.073 Å has been observed between the 0_0 and 0_1 conformations. The corresponding change in P_1 =N_2 bond length is 0.057 Å. Similarly to the "single" N_1 P_1 bond, the "double" P_1 =N_2 bond is longest near sulfur in all conformations. While N_1 P_1 and P_1=N_2 bond lengths show substantial variations between conformations, the differences between them within a given conformation remain relatively constant (approximately 0.1 Å) in all conformations. Both the 0_0 and 0_3 conformations are different from other conformations in that, while the "double" bond P_1 =N_2 is shorter than the "single" N_1 P_1 bond, it is actually longer than the "single" bond N_2-P_2 following it. In effect, in these

conformations, the "single-double" pattern has been replaced by decreasing bond lengths along the backbone with the increasing distance of nitrogen or phosphorus away from the sulfur. The remaining bond lengths are relatively unaffected by the conformational changes (see table (3.1)).

The main observation that can be made about bond angles in model 1 compound (see table (3.2)) is that bond angles along the backbone: $S_1N_1P_1$, $N_1P_1N_2$, $P_1N_2P_2$ and $N_2P_2N_3$ open up at the same time as the rotation around N_1–P_1 bond is performed. This is especially true for $S_1N_1P_1$ angle which increases on the average by 11°. The openings of $P_1N_2P_2$ and $N_2P_2N_3$ bond angles are of comparable magnitudes ($\approx$ 10°) with the exception in the 0_2 conformation which is closer to 5°. The magnitude of $N_1P_1N_2$ increases on the average by 4°. The HPN bond angles on P_1 also increase by a few degrees. In contrast the HPN bond angles on P_2 decrease by a similar amount. The $O_1S_1N_1$ bond angle remains relatively insensitive to the rotations, its average value is approximately 124°. The $C_1S_1N_1$ also remained close to 110°. There is some variation in the $C_2N_3P_2$ with some decreases or some increases by a few degrees depending on the conformation.

In the case of dihedral angles (see table (3.3)), we note that the rotation around the N_1-P_1 is strongly coupled to another rotational mode, that is to the simultaneous rotation around N_3-P_2 bond as is exhibited by the values of C_2N_3–P_2N_2 dihedral angles. These dihedral angles can deviate substantially from the expected 180° (e.g. in the global minimum the deviation is 37°). Smaller deviations from the expected values of 180° and 0° have also been observed in P_2N_2–P_1N_1 and N_3P_2–N_2P_1 dihedral angles. The position of the oxygen relative to backbone is also readjusted by 10° to 20° depending on the conformation.

For the hydrogenated model 2 compound with R^1=Cl we have also found four local minima besides the the global one (see tables (3.5–3.8)). Similar to the model 1 compound

we have found either bond length alternation pattern or decreasing bond lengths (in the 0_0 and 0_3 conformations) along the backbone (see in table (3.5)). In the alternating case, the "single" and "double" bonds are longer near S_1. We note that the bond lengths are less sensitive to the rotation around the N_1-P_1 bond in comparison to the similar results for the model 1 compound. For example, a difference of 0.01 Å has been observed between N_1-P_1 bonds in the 0_0 and 0_1 conformations (the largest difference of 0.04 Å has been observed between other conformations). The remaining bond lengths are relatively unaffected by the conformational changes (see table (3.5)).

Also in comparison to the model 1 compound, we see from table 3.6 that there are smaller bond angle openings in the bond angles along the backbone (the largest opening is of the order of 8° in 0_2 conformation in the $P_1N_2P_2$ bond angle). These smaller changes in the bond angles between conformations are reflected in the correspondingly smaller variations in the bond lengths.

In agreement with the above trend, the dihedral angles (see table (3.7)) are also relatively unaffected by the rotation. However, similar to the model 1 compound, we also observe some coupling between the N_2P_1-N_1S_1 and the C_2N_3 P_2N_2 dihedral angles. Except for the 0_2 conformation, the deviations of C_2N_3-P_2N_2 dihedral angle from the expected value of 180° are approximately +/−30°. We conclude this subsection, by stated that the presence of F on S in comparison to having Cl on S, leads to more structural relaxations in the chain. We base this conclusion on the observation that the rotation in model 1 compound results in greater number of distortions of larger magnitudes than in model 2 compound.

Table 3.1: Comparison of bond lengths (Å) for the global (0_0) and the local minima (0_k,k=1–4) of PTPs with R^1=F and R^2_n=H, (n=1–4).

Bond	0_0	0_1	0_2	0_3	0_4
$O_1=S_1$	1.460	1.451	1.455	1.458	1.453
$S_1=N_1$	1.516	1.507	1.506	1.505	1.511
N_1-P_1	1.766	1.694	1.725	1.751	1.703
$P_1=N_2$	1.653	1.596	1.614	1.650	1.592
N_2-P_2	1.629	1.642	1.637	1.631	1.640
$P_2=N_3$	1.619	1.585	1.591	1.616	1.583
R^1-S_1	1.650	1.647	1.647	1.657	1.648
C_1-S_1	1.772	1.757	1.761	1.764	1.758
$R^2_1-P_1$	1.430	1.422	1.427	1.425	1.431
$R^2_2-P_1$	1.417	1.428	1.421	1.427	1.428
$R^2_3-P_2$	1.434	1.442	1.444	1.445	1.447
$R^2_4-P_2$	1.446	1.452	1.445	1.435	1.449
H_1-C_1	1.103	1.102	1.103	1.103	1.103
H_2-C_1	1.101	1.103	1.102	1.101	1.102
H_3-C_1	1.100	1.100	1.101	1.100	1.100
C_2-N_3	1.439	1.445	1.437	1.438	1.443
H_4-C_2	1.115	1.119	1.113	1.110	1.114
H_5-C_2	1.109	1.108	1.109	1.113	1.107
H_6-C_2	1.110	1.114	1.112	1.114	1.117

Table 3.2: Comparison of bond angles (degrees) for the global (0_0) and the local minima (0_k,k=1-4) of PTPs with R^1=F and R^2_n=H, (n=1-4).

Bond angle	0_0	0_1	0_2	0_3	0_4
$\angle O_1S_1N_1$	122.900	125.362	124.347	123.933	124.310
$\angle S_1N_1P_1$	116.321	129.698	126.839	124.918	125.662
$\angle N_1P_1N_2$	100.115	105.710	103.044	101.238	103.029
$\angle P_1N_2P_2$	98.036	109.076	103.650	97.894	109.984
$\angle N_2P_2N_3$	97.953	107.590	101.944	98.852	107.413
$\angle R^2_2P_1N_1$	92.124	106.363	95.737	90.461	103.824
$\angle R^2_3P_2N_2$	111.820	104.555	109.040	115.866	107.325
$\angle R^2_4P_2N_2$	115.076	111.027	110.908	111.632	106.907
$\angle H_1C_1S_1$	106.050	106.119	106.103	106.225	105.159
$\angle H_2C_1S_1$	108.013	106.916	107.216	107.398	107.614
$\angle H_3C_1S_1$	108.977	108.472	108.754	108.468	109.445
$\angle C_2N_3P_2$	127.777	120.854	131.821	127.952	122.579
$\angle H_4C_2N_3$	114.230	113.814	113.619	113.188	113.720
$\angle H_5C_2N_3$	108.463	109.918	108.754	108.234	109.859
$\angle H_6C_2N_3$	112.785	113.681	113.636	114.329	113.459

Table 3.3: Comparison of dihedral angles (degrees) for the global (0_0) and the local minima (0_k,k=1-4) of PTPs with R^1=F and R^2_n=H, (n=1-4).

Dihedral angle	0_0	0_1	0_2	0_3	0_4
$\angle P_1N_1\text{-}S_1O_1$	-31.850	-11.849	-12.885	-21.397	-20.782
$\angle N_2P_1\text{-}N_1S_1$	-58.297	93.404	241.773	276.040	176.911
$\angle P_2N_2\text{-}P_1N_1$	173.535	164.146	-174.009	-168.948	-178.560
$\angle N_3P_2\text{-}N_2P_1$	11.364	10.060	0.054	-6.222	8.005
$\angle R^1S_1\text{-}N_1O_1$	123.834	123.304	124.556	125.790	123.735
$\angle C_1S_1\text{-}N_1R^1$	103.202	100.976	101.505	101.955	101.772
$\angle R^2_1P_1\text{-}N_1N_2$	124.317	125.822	126.530	123.531	124.944
$\angle R^2_2P_1\text{-}N_1R^2_1$	109.517	108.351	108.327	109.564	108.168
$\angle R^2_3P_2\text{-}N_2N_3$	126.096	130.043	126.468	120.654	127.221
$\angle R^2_4P_2\text{-}N_2R^2_3$	113.739	106.091	108.108	113.966	105.249
$\angle H_1C_1\text{-}S_1O_1$	49.620	51.235	59.776	53.507	51.298
$\angle H_2C_1\text{-}S_1H_1$	-118.726	-119.002	-118.577	-118.621	-118.360
$\angle H_3C_1\text{-}S_1H_1$	119.661	120.538	120.111	120.175	119.820
$\angle C_2N_3\text{-}P_2N_2$	217.076	203.820	189.422	136.011	173.171
$\angle H_4C_2\text{-}N_3P_2$	38.526	45.758	43.973	108.605	72.713
$\angle H_5C_2\text{-}N_3C_2$	119.343	119.181	118.346	117.966	119.287
$\angle H_6C_2\text{-}N_3C_2$	-123.575	-122.553	-123.422	-123.743	-122.006

Table 3.4: Comparison of the total energies (hartrees) and corresponding energy differences (given in hartrees and kcal/mole) for the global (0_0) and the local minima (0_k,k=1 4) of PTPs with R^1=F and R^2_n=H, (n=1-4).

minimum	E_{total}(har)	$\angle N_2P_1\text{-}N_1S_1$	$\angle C_2N_3\text{-}P_2N_2$	ΔE(har)	ΔE(kcal/mole)
0_0	-1495.249487	-58.297	217.076	—	—
0_1	-1495.247703	93.404	203.820	0.0018	1.1
0_2	-1495.247671	241.773	189.422	0.0018	1.1
0_3	-1495.247272	276.040	136.011	0.0022	1.4
0_4	-1495.245928	176.911	173.171	0.0036	2.3

Table 3.5: Comparison of bond lengths (Å) for the global (0_0) and the local minima (0_k,k=1–4) of PTPs with R^1=Cl and R^2_n=H, (n=1–4).

Bond	0_0	0_1	0_2	0_3	0_4
O_1=S_1	1.466	1.466	1.457	1.475	1.465
S_1=N_1	1.521	1.516	1.532	1.516	1.523
N_1–P_1	1.753	1.763	1.718	1.764	1.719
P_1=N_2	1.652	1.648	1.611	1.648	1.605
N_2–P_2	1.630	1.630	1.638	1.628	1.639
P_2=N_3	1.616	1.612	1.591	1.611	1.590
R^1–S_1	2.155	2.185	2.135	2.196	2.148
C_1–S_1	1.771	1.765	1.773	1.773	1.769
R^2_1–P_1	1.426	1.418	1.425	1.438	1.428
R^2_2–P_1	1.426	1.431	1.419	1.423	1.422
R^2_3–P_2	1.443	1.445	1.443	1.435	1.443
R^2_4–P_2	1.434	1.436	1.447	1.444	1.447
H_1–C_1	1.103	1.103	1.104	1.103	1.104
H_2–C_1	1.105	1.104	1.104	1.103	1.104
H_3–C_1	1.101	1.101	1.099	1.102	1.101
C_2–N_3	1.435	1.440	1.440	1.436	1.438
H_4–C_2	1.111	1.111	1.114	1.112	1.113
H_5–C_2	1.111	1.109	1.107	1.112	1.108
H_6–C_2	1.113	1.113	1.113	1.109	1.113

Table 3.6: Comparison of bond angles (degrees) for the global (0_0) and the local minima (0_k, k=1-4) of PTPs with R^1=Cl and R^2_n=H, (n=1-4).

Bond angle	0_0	0_1	0_2	0_3	0_4
$\angle O_1S_1N_1$	124.666	124.428	123.61	125.960	125.122
$\angle S_1N_1P_1$	122.595	119.399	119.21	123.032	124.600
$\angle N_1P_1N_2$	98.268	96.615	104.21	95.323	96.425
$\angle N_2P_2N_3$	96.732	97.715	102.67	97.228	98.359
$\angle R^1N_1S_1$	113.059	111.454	111.43	109.029	109.930
$\angle C_1S_1N_1$	105.319	107.747	107.52	107.437	106.853
$\angle R^2_1P_1N_1$	96.351	93.865	101.63	94.739	98.300
$\angle R^2_2P_1N_1$	91.256	97.511	97.72	97.573	94.078
$\angle R^2_3P_2N_2$	115.433	115.190	108.57	111.816	111.582
$\angle R^2_4P_2N_2$	112.927	111.474	109.88	115.175	116.182
$\angle H_1C_1S_1$	106.917	106.343	105.27	106.800	107.406
$\angle H_2C_1S_1$	106.078	106.044	106.17	108.011	107.653
$\angle H_3C_1S_1$	109.260	108.837	110.66	107.901	107.436
$\angle C_2N_3P_2$	133.394	129.512	127.14	133.377	125.621
$\angle H_4C_2N_3$	113.145	112.673	113.96	113.789	113.806
$\angle H_5C_2N_3$	107.644	108.813	109.15	108.225	109.000
$\angle H_6C_2N_3$	114.193	113.881	113.30	112.863	112.671

Table 3.7: Comparison of dihedral angles (Å) for the global (0_0) and the local minima (0_k,k=1-4) of PTPs with R^1=Cl and R^2_n=H, (n=1-4).

Dihedral angle	0_0	0_1	0_2	0_3	0_4
$\angle P_1N_1\text{-}S_1O_1$	-33.883	-30.400	-51.520	-56.860	65.541
$\angle N_2P_1\text{-}N_1S_1$	-48.625	95.901	-21.702	185.769	249.472
$\angle P_2N_2\text{-}P_1N_1$	-172.305	-175.960	-176.511	171.743	175.476
$\angle N_3P_2\text{-}N_2P_1$	-5.002	-6.562	3.000	6.036	9.955
$\angle R^1S_1\text{-}N_1O_1$	127.207	122.991	127.511	124.961	125.251
$\angle C_1S_1\text{-}N_1R^1$	105.776	105.670	106.920	102.402	103.467
$\angle R^2_1P_1\text{-}N_1N_2$	123.835	123.779	125.413	126.904	125.602
$\angle R^2_2P_1\text{-}N_1R^2_1$	107.741	108.623	107.701	108.474	108.678
$\angle R^2_3P_2\text{-}N_2N_3$	120.905	120.995	126.710	125.063	126.753
$\angle R^2_4P_2\text{-}N_2R^2_3$	114.634	113.408	107.423	113.707	114.288
$\angle H_1C_1\text{-}S_1O_1$	51.129	50.844	49.800	48.423	45.619
$\angle H_2C_1\text{-}S_1H_1$	-118.762	-118.977	-117.112	-120.188	120.418
$\angle H_3C_1\text{-}S_1H_1$	120.981	120.439	120.702	119.438	119.830
$\angle C_2N_3\text{-}P_2N_2$	148.096	154.725	181.586	210.822	216.277
$\angle H_4C_2\text{-}N_3P_2$	89.644	83.305	57.000	23.045	22.708
$\angle H_5C_2\text{-}N_3C_2$	117.202	117.674	118.818	118.401	118.643
$\angle H_6C_2\text{-}N_3C_2$	-124.033	-123.007	-122.809	-123.917	-123.181

Table 3.8: Comparison of total energies (hartrees) and corresponding energy differences (given in hartrees and kcal/mole) for the global (0_0) and the local minima (0_k,k=1-4) of PTPs with R^1=Cl and R^2_n=H, (n=1-4).

minimum	E_{total}(har)	$\angle N_2P_1\text{-}N_1S_1$	$\angle C_2N_3\text{-}P_2N_2$	ΔE(har)	ΔE(kcal/mole)
0_0	-1854.694374	-48.625	148.096	...	
0_1	-1854.693458	95.901	154.725	0.0009	0.6
0_2	-1854.691903	-21.702	181.586	0.0025	1.6
0_3	-1854.689616	185.769	210.822	0.0048	3.0
0_4	-1854.688636	249.472	216.277	0.0057	3.6

(ii) Chlorine Substituted Model Compounds

We have found fewer minima for the chlorinated model compounds. In the case of model 3 compound (with R'=F) we have obtained three local minimum structures in addition to the global minimum. No significant variations (less than 0.02 Å) in the bond lengths have been observed between the four conformations due to rotation around N_1–P_1 bond (see table (3.9)). The "single-double" bond alternation along the chain backbone is clearly distinguishable. Within a given conformation the difference between the "single" and "double" bonds is approximately 0.1 Å.

Similarly to what has been observed in the model 1 compound, bond angle openings accompany the rotation around the N_1–P_1 bond (see table (3.10)) in model 3 compound. The $S_1N_1P_1$ bond angle increases by 7.5° in the 0_1 conformation relative to the 0_0 conformation. The corresponding increase of 10° is observed in the 0_3 conformation. A small decrease (1.2°) has been observed in the 0_2 conformation, this decrease is accompanied by an opening of $P_1N_2P_2$ bond angle by 13.9° relative to the 0_0 conformation. The remaining bond angles are relatively insensitive to the rotation.

In the model 3 compound, in the three lowest minima (0_0, 0_1 and 0_2) the coupling between the N_2P_1-N_1S_1 and the C_2N_3-P_2N_2 dihedral angles is not as pronounced (see table (3.11)) as in the hydrogen substituted compounds. In these cases C_2N_3-P_2N_2 dihedral angles are close to 180°, only in the 0_3 conformation this angle deviates by 28° from the expected value of 180°. Some variations (of the order of few degrees) has been observed in the P_2N_2-P_1N_1 and N_3P_2-N_2P_1 dihedral angles along the chain backbone indicating that the torsional rotation results in a more twisted structure in comparison to the global minimum structure.

In the model 4 compound (with R'=Cl) we have found three local minima in addition to the global minimum. Similar to the model 3 compound, the bond lengths remain

relatively unchanged during the torsional rotation around the N_1–P_1 bond (see table (3.13)). In fact, the changes are smaller than in the model 3 compound. Within a given conformation the "single–double" bond alternation along the chain backbone is also present in this compound and the difference between the "single" and "double" bonds is approximately 0.1 Å (as in model 3 compound).

The $S_1N_1P_1$ bond angle opening also occurs for this compound upon rotation (see table (3.14)). However, a significant increase is not observed till the third lowest local minimum (0_2). In that case the $S_1N_1P_1$ bond angle opens up by 11° in the 0_2 conformation and by 16° in 0_3 conformation. In contrast, to the model 3 compound, the $S_1N_1P_1$ bond angle opening is accompanied by the $P_1N_2P_2$ bond angle closing (by 7.6° and 4.3° in the respective conformations).

The coupling between the two dihedral angles: the N_2P_1-N_1S_1 and the C_2N_3-P_2N_2 is also present in this model compound (see table (3.15)). In the local minima structures, C_2N_3–P_2N_2 differs approximately by ± 10° in comparison to the global minimum structure. Other dihedral angles exhibit some changes upon rotation. The largest variation has been observed in the N_3P_2–N_2P_1 dihedral angle in 0_1 conformation which increases by 27° relative to the 0_0 conformation. Again this illustrates the point that rotation around N_1–P_1 bond leads to relaxations of other dihedral angles along the backbone.

We conclude this subsection by pointing out that in the model compound 3 and 4, the torsion around N_1–P_1 bond results in $S_1N_1P_1$ bond angle openings with model 3 compound exhibiting larger opening in 0_1 conformation. In the case of model compound 4, concurrent closings of $P_1N_2P_2$ bond angles also occurred. The coupling between the N_2P_1–N_1S_1 and the C_2N_3-P_2N_2 dihedral angles is present again with somewhat larger deviations observed in model 3 compound. Overall greater distortions along the backbone occur in the model 3 compound. Based on this structural analysis we would conclude again that more structural relaxations are present in the model 4 compound than in the

model 3 due to the rotation. However, this difference is not as clearly defined as in the hydrogenated model compounds (see above).

Table 3.9: Comparison of bond lengths (Å) for the global (0_0) and the local minima (0_k,k=1-3) of PTPs with R^1=F and R^2_n=Cl, (n=1-4).

Bond	0_0	0_1	0_2	0_3
O_1=S_1	1.443	1.446	1.443	1.452
S_1=N_1	1.537	1.525	1.539	1.527
N_1–P_1	1.662	1.655	1.660	1.653
P_1=N_2	1.566	1.557	1.545	1.565
N_2–P_2	1.642	1.634	1.622	1.639
P_2=N_3	1.544	1.539	1.541	1.536
R^1–S_1	1.614	1.635	1.617	1.629
C_1–S_1	1.758	1.756	1.761	1.763
R^2_1–P_1	2.041	2.034	2.023	2.047
R^2_2–P_1	2.024	2.039	2.038	2.036
R^2_3–P_2	2.088	2.075	2.079	2.074
R^2_4–P_2	2.076	2.081	2.093	2.083
H_1–C_1	1.105	1.104	1.105	1.102
H_2–C_1	1.103	1.103	1.102	1.104
H_3–C_1	1.100	1.101	1.100	1.102
C_2–N_3	1.437	1.437	1.444	1.432
H_4–C_2	1.110	1.111	1.111	1.114
H_5–C_2	1.106	1.107	1.105	1.109
H_6–C_2	1.110	1.110	1.111	1.108

Table 3.10: Comparison of bond angles (degrees) for the global (0_0) and the local minima (0_k,k=1 3) of PTPs with R^1=F and R^2_n=Cl, (n=1–4).

Bond angle	0_0	0_1	0_2	0_3
$\angle O_1S_1N_1$	123.577	123.739	123.516	126.330
$\angle S_1N_1P_1$	118.624	126.170	117.364	128.572
$\angle N_1P_1N_2$	110.923	106.967	109.094	106.416
$\angle P_1N_2P_2$	121.532	122.587	135.401	119.350
$\angle N_2P_2N_3$	112.481	112.899	116.019	111.431
$\angle R^1N_1S_1$	107.679	106.780	104.532	105.528
$\angle C_1S_1N_1$	108.602	109.086	111.117	104.843
$\angle R^2_1P_1N_1$	104.974	108.912	101.461	106.885
$\angle R^2_2P_1N_1$	101.541	103.576	108.376	105.995
$\angle R^2_3P_2N_2$	104.158	105.765	102.937	103.195
$\angle R^2_4P_2N_2$	104.327	102.410	102.319	107.266
$\angle H_1C_1S_1$	105.239	105.120	104.985	107.849
$\angle H_2C_1S_1$	106.735	106.523	107.930	106.420
$\angle H_3C_1S_1$	110.373	110.448	108.323	109.091
$\angle C_2N_3P_2$	128.582	128.559	124.883	130.545
$\angle H_4C_2N_3$	112.202	112.602	112.684	113.700
$\angle H_5C_2N_3$	108.713	108.834	108.991	107.901
$\angle H_6C_2N_3$	112.894	112.388	112.585	111.926

Table 3.11: Comparison of dihedral angles (degrees) for the global (0_0) and the local minima (0_k,k=1-3) of PTPs with R^1=F and R^2_n=Cl, (n=1-4).

Dihedral angle	0_0	0_1	0_2	0_3
$\angle P_1N_1-S_1O_1$	-37.215	-44.311	-13.053	-54.692
$\angle N_2P_1-N_1S_1$	-42.681	223.296	59.034	194.824
$\angle P_2N_2-P_1N_1$	-176.380	168.781	172.558	161.751
$\angle N_3P_2-N_2P_1$	-5.954	10.052	26.117	14.682
$\angle R^1S_1-N_1O_1$	123.229	124.026	120.712	122.001
$\angle C_1S_1-N_1R^1$	104.940	105.312	102.118	105.743
$\angle R^2_1P_1-N_1N_2$	126.883	126.807	125.335	127.213
$\angle R^2_2P_1-N_1R^2_1$	107.042	109.541	107.944	108.374
$\angle R^2_3P_2-N_2N_3$	126.740	128.184	128.970	129.793
$\angle R^2_4P_2-N_2R^2_3$	103.434	103.960	102.074	104.335
$\angle H_1C_1-S_1O_1$	53.270	48.354	44.153	54.612
$\angle H_2C_1-S_1H_1$	-117.484	-117.166	-118.165	-118.779
$\angle H_3C_1-S_1H_1$	120.349	121.084	119.304	122.047
$\angle C_2N_3-P_2N_2$	179.677	174.371	175.525	208.139
$\angle H_4C_2-N_3P_2$	71.890	68.820	64.124	14.024
$\angle H_5C_2-N_3C_2$	118.437	118.761	119.285	119.192
$\angle H_6C_2-N_3C_2$	-122.353	-122.388	-121.598	-122.711

Table 3.12: Comparison of the total energies (hartrees) and corresponding energy differences (given in hartrees and kcal/mole) for the global (0_0) and the local minima (0_k,k=1-3) of PTPs with R^1=F and R^2_n=Cl, (n=1-4).

minimum	E_{total}(har)	$\angle N_2P_1-N_1S_1$	$\angle C_2N_3-P_2N_2$	ΔE(har)	ΔE(kcal/mole)
0_0	-3327.7945477	-42.681	179.677		
0_1	-3327.7912147	223.296	174.371	0.0033	2.1
0_2	-3327.7907790	59.034	175.525	0.0038	2.4
0_3	-3327.7871092	194.824	208.139	0.0074	4.7

Table 3.13: Comparison of bond lengths (Å) for the global (0_0) and the local minima (0_k,k=1–3) of PTPs with R^1=Cl and R^2_n=Cl, (n=1–4).

Bond	0_0	0_1	0_2	0_3
$O_1=S_1$	1.453	1.450	1.462	1.460
$S_1=N_1$	1.554	1.551	1.542	1.530
N_1-P_1	1.661	1.660	1.651	1.645
$P_1=N_2$	1.560	1.562	1.565	1.561
N_2-P_2	1.636	1.637	1.639	1.634
$P_2=N_3$	1.536	1.539	1.538	1.542
R^1-S_1	2.100	2.120	2.119	2.122
C_1-S_1	1.770	1.760	1.771	1.773
$R^2_1-P_1$	2.027	2.021	2.04	2.042
$R^2_2-P_1$	2.034	2.035	2.039	2.030
$R^2_3-P_2$	2.072	2.070	2.081	2.082
$R^2_4-P_2$	2.094	2.090	2.075	2.076
H_1-C_1	1.105	1.104	1.103	1.102
H_2-C_1	1.104	1.106	1.105	1.105
H_3-C_1	1.101	1.100	1.101	1.102
C_2-N_3	1.435	1.438	1.435	1.440
H_4-C_2	1.110	1.110	1.112	1.112
H_5-C_2	1.106	1.107	1.108	1.107
H_6-C_2	1.110	1.110	1.109	1.109

Table 3.14: Comparison of bond angles (degrees) for the global (0_0) and the local minima (0_k,k=1-3) of PTPs with R^1=Cl and R^2_n=Cl, (n=1-4).

Bond angle	0_0	0_1	0_2	0_3
$\angle O_1S_1N_1$	120.656	123.456	123.495	123.447
$\angle S_1N_1P_1$	116.969	119.091	128.271	132.959
$\angle N_1P_1N_2$	109.659	110.584	105.353	107.667
$\angle P_1N_2P_2$	127.426	122.264	118.866	123.131
$\angle N_2P_2N_3$	112.718	112.930	111.519	113.533
$\angle R^1N_1S_1$	110.753	109.442	108.851	108.994
$\angle C_1S_1N_1$	106.719	106.164	104.360	103.233
$\angle R^2_1P_1N_1$	105.837	101.705	106.260	109.205
$\angle R^2_2P_1N_1$	102.674	106.230	107.075	102.956
$\angle R^2_3P_2N_2$	103.473	102.529	104.087	101.775
$\angle R^2_4P_2N_2$	104.605	105.051	105.436	104.956
$\angle H_1C_1S_1$	105.424	105.556	106.505	107.407
$\angle H_2C_1S_1$	106.393	105.331	106.466	105.950
$\angle H_3C_1S_1$	110.223	110.963	109.231	108.811
$\angle C_2N_3P_2$	130.705	128.757	131.217	128.331
$\angle H_4C_2N_3$	112.523	112.575	113.350	113.424
$\angle H_5C_2N_3$	108.389	108.593	108.780	108.811
$\angle H_6C_2N_3$	112.593	112.559	112.051	111.621

Table 3.15: Comparison of dihedral angles (degrees) for the global (0_0) and the local minima (0_k,k=1–3) of PTPs with R^1=Cl and R^2_n=Cl, (n=1–4).

Dihedral angle	0_0	0_1	0_2	0_3
$\angle P_1N_1\text{-}S_1O_1$	-51.983	-26.643	-48.726	-55.460
$\angle N_2P_1\text{-}N_1S_1$	-29.711	49.418	178.971	233.941
$\angle P_2N_2\text{-}P_1N_1$	179.277	179.575	174.172	-174.298
$\angle N_3P_2\text{-}N_2P_1$	1.741	29.175	-5.358	6.334
$\angle R^1S_1\text{-}N_1O_1$	126.562	124.887	126.841	126.281
$\angle C_1S_1\text{-}N_1R^1$	107.775	108.082	104.910	106.038
$\angle R^2_1P_1\text{-}N_1N_2$	127.041	123.608	125.601	127.197
$\angle R^2_2P_1\text{-}N_1R^2_1$	107.294	108.130	109.073	108.633
$\angle R^2_3P_2\text{-}N_2N_3$	127.526	129.621	129.167	129.299
$\angle R^2_4P_2\text{-}N_2R^2_3$	103.084	104.024	103.721	103.170
$\angle H_1C_1\text{-}S_1O_1$	52.861	52.224	52.217	49.622
$\angle H_2C_1\text{-}S_1H_1$	-117.519	-116.546	-118.470	-119.150
$\angle H_3C_1\text{-}S_1H_1$	120.343	122.339	120.754	121.289
$\angle C_2N_3\text{-}P_2N_2$	181.700	-172.651	192.033	190.281
$\angle H_4C_2\text{-}N_3P_2$	65.473	51.394	32.337	28.120
$\angle H_5C_2\text{-}N_3C_2$	118.538	119.059	118.676	118.964
$\angle H_6C_2\text{-}N_3C_2$	-122.450	-122.379	-122.642	-122.487

Table 3.16: Comparison of the total energies (hartrees) and corresponding energy differences (given in hartrees and kcal/mole) for the global (0_0) and the local minima (0_k,k=1–4) of PTPs with R^1=Cl and R^2_n=Cl, (n=1–4).

minimum	E_{tot}(har)	$\angle N_2P_1\text{-}N_1S_1$	$\angle C_2N_3\text{-}P_2N_2$	ΔE(har)	ΔE(kcal/mole)
0_0	-3687.2363355	-29.711	181.700	—	—
0_1	3687.2352704	49.418	-172.651	0.0011	0.7
0_2	3687.2321303	178.971	192.033	0.0042	2.6
0_3	3687.2310020	233.941	190.281	0.0053	3.3

(iii) Model compounds with one more $NP(Cl_2)$ group.

We have investigated the global minima of two other model compounds with one extra $NP(Cl_2)$ group in between sulfur atom and the end group along the backbone, (extended backbone chain) with R^1=F (model 5) and R^1=Cl (model 6). We hope these extended models are closer to the polymer structure than the model compounds 3 and 4. In order to focus on the structural differences between model compounds 3-4 and 5-6, we compare the geometrical parameters of model compound 5 with those of model compound 3, and model compound 6 with those of model compound 4. Model 5-6 compounds also allow us to investigate the NSN bond angle and SN single bond length.

No significant variations (less than 0.02 Å) in the bond lengths have been observed between the global minima of model 3 and model 5 compounds. The "single-double" bond alternation along the chain backbone is clearly distinguishable in model compound 5, as usual in the chlorinated compounds. The difference between the "single" and "double" bonds is approximately 0.1 Å. The "single" N_1-P_1 and "double" P_3=N_4 bonds are longer near sulfur. We note that the bond lengths are relatively unaffected by the lengthening of the backbone chain.

In comparison to the model compound 3, we see from table (3.17) that there is an increase in the bond angle $S_1N_1P_1$ by 8°. Both $S_1N_1P_1$ and $P_3N_4S_1$ are of similar magnitudes (~127°). The value of the NSN bond angle (107°) is close to the tetrahedral angle. The bond angles $R_5^2P_3N_4$ and $R_6^2P_3N_4$ increase by 10° for model 5 compound, which was not observed in the first four model compounds. The remaining of the bond angles are nearly the same as those of model 3 compound (differences are less than 2°).

Most of the dihedral angles along the backbone are readjusted by the inclusion of $NP(Cl_2)$ group. For example, in comparison to model 3, in model 5 compound the dihedral angle O_1S_1-N_1P_1 decreases by 23.5°, N_2P_1 N_1S_1 increases by 8°, P_2N_2 P_1N_1

increases by 8°, and N_3P_2–N_1P_1 increases by 32°. The dihedral angles N_4S_1–N_1P_1 and P_3N_4 S_1N_1 deviated from their expected values by 14° and 7° respectively. Positions of the substituents relative to the backbone are not affected by the extra $NP(Cl_2)$ group.

When model 6 and model 4 compounds are compared, it can be seen that, bond lengths remain almost unaffected by the presence of extra group along the backbone. In both models 4 and 6 the "single-double" bond alternation along the chain backbone is very similar. The difference between the "single" and "double" bonds are approximately 0.1 Å. Similar to the model compound 4, the "single" and "double" bonds are longer near sulfur. There is no change in the $S_1N_1P_1$ bond angle. But in agreement with the above trend, in model 6, the bond angles $R^2_5P_3N_4$ and $R^2_6P_3N_4$ increase by 10° in comparison to the R^2PN bond angles in model 4. The remaining bond angles are almost the same as those in model 4 compound.

We observe many differences in the dihedral angles between the model 4 and model 6 compounds. In model 6 compound almost all dihedral angles along the backbone increase by a few degrees. For example, the dihedral angles O_1S_1–N_1P_1 increases by 5°, N_2P_1–N_1S_1 by 5.2°, P_2 N_2–P_1N_1 by 12° and N_3P_2–N_1P_1 by 16.5°. Other two angles N_4S_1–N_1P_1 and P_3N_4–S_1N_1 deviated from their expected values 180° and 0° by 9° and 18° respectively. This could compensate for the increase in the bond angles $R^2_5P_3N_4$ and $R^2_6P_3N_4$ as noted above. This distortion is expected in the presence of sulfur. Positions of the substituents (R^2 atoms) are not affected by the extra $NP(Cl_2)$ group.

We conclude this subsection by pointing out that, the extended model compounds exhibit similar structures as the short model compounds (the end groups have no significant effect on the structures).

Table 3.17: Comparison of **(a)** bond lengths (Å), and **(b)** bond angles (degrees) of extended PTPs with R^1=Cl, F and R^2_n=Cl, (n=1-6).

(a)

Bond	model 5 R^1=F	model 6 R^1=Cl
$S_1=O_1$	1.443	1.447
$S_1=N_1$	1.546	1.570
N_1-P_1	1.645	1.658
$P_1=N_2$	1.569	1.556
N_2-P_2	1.640	1.624
$P_2=N_3$	1.539	1.537
S_1-R^1	1.599	2.093
$N_4=S_1$	1.599	1.608
$P_3=N_4$	1.573	1.578
$P_1-R^1_2$	2.041	2.044
$P_1-R^2_2$	2.033	2.016
$P_2-R^3_2$	2.081	2.084
$P_2-R^4_2$	2.088	2.084
$P_3-R^5_2$	2.031	2.025
$P_3-R^6_2$	2.034	2.032
P_3-C_2	1.573	1.578
N_3-C_1	1.435	1.436
C_1-H_1	1.110	1.110
C_1-H_2	1.107	1.108
C_1-H_3	1.110	1.110
C_2-H_4	1.106	1.106
C_2-H_5	1.105	1.104
C_2-H_6	1.101	1.103

(b)

Bond Angle	model 5 R^1=F	model 6 R^1=Cl
$\angle O_1S_1N_1$	123.951	118.920
$\angle S_1N_1P_1$	126.526	114.458
$\angle N_1P_1N_2$	113.023	109.429
$\angle P_1N_2P_2$	120.445	131.181
$\angle N_2P_2N_3$	111.866	113.043
$\angle R^1S_1N_1$	106.631	110.077
$\angle C_1N_3P_2$	131.853	129.846
$\angle N_4S_1N_1$	107.040	107.026
$\angle P_3N_4S_1$	128.549	125.563
$\angle R^2_1P_1N_1$	107.304	106.889
$\angle R^2_2P_1N_1$	99.860	103.849
$\angle R^2_3P_2N_2$	102.159	100.061
$\angle R^2_4P_2N_2$	105.978	107.263
$\angle R^2_5P_3N_4$	114.482	116.808
$\angle R^2_6P_3N_4$	117.364	114.619
$\angle H_1C_1N_3$	113.799	113.654
$\angle H_2C_1H_1$	107.518	107.618
$\angle H_3C_1H_1$	108.157	108.021
$\angle C_2P_3N_4$	105.310	106.626
$\angle H_4C_2N_3$	106.929	107.541
$\angle H_5C_2N_3$	108.918	109.419
$\angle H_6C_2N_3$	110.853	110.516

Table 3.18: Comparison of (c) dihedral angles(degrees) of extended PTPs with R^1=Cl, F and R^2_n=Cl, (n=1-6).

(c)

Dihedral angle	model 5 R^1=F	model 6 R^1=Cl
$\angle O_1S_1-N_1P_1$	-60.718	-43.189
$\angle N_2P_1-N_1S_1$	-34.52	-24.182
$\angle P_2N_2-P_1N_1$	177.520	-167.677
$\angle N_3P_2-N_2P_1$	25.931	17.308
$\angle R^1S_1-N_1O_1$	122.420	124.317
$\angle C_1N_3-P_2N_2$	-170.484	-171.713
$\angle N_4S_1-N_1P_1$	166.352	-171.180
$\angle P_3N_4-S_1N_1$	7.085	17.996
$\angle R^2_1P_1-N_1N_2$	128.014	124.481
$\angle R^2_2P_1-N_1R^2_1$	106.566	107.553
$\angle R^2_3P_2-N_2N_3$	130.542	129.602
$\angle R^2_4P_2-N_2R^2_3$	102.380	102.021
$\angle R^2_5P_3-N_4S_1$	69.058	42.424
$\angle R^2_6P_3-N_4S_1$	-52.486	-80.353
$\angle H_1C_1-N_3P_2$	25.349	25.532
$\angle H_2C_1-H_1N_3$	-120.210	-120.301
$\angle H_3C_1-H_1N_3$	-115.407	-115.764
$\angle C_2P_3-N_4S_1$	-173.281	160.986
$\angle H_4C_2-P_3N_4$	-47.879	-64.386
$\angle H_5C_2-H_4P_3$	-116.202	-116.986
$\angle H_6C_2-H_4P_3$	-121.909	-122.092

3.2 Conformational Analysis

In this section we examine the locations and the energies of the local minima relative to the global minimum in the PTPs model compounds. In the above sections the structural changes between conformations have been discussed. This structural analysis points to the fact that the multidimensional CPES has a complicated structure. The main observations can be summarized as follows: (1) some variations of bond lengths have been noted with greater changes observed in the compounds with R^1=F; (2) the openings of the backbone bond angles upon rotation are present in all model compounds; (3) a number of dihedral angle couplings have occurred, we especially noted the coupling between the N_2P_1–N_1S_1 and the C_2N_3–P_2N_2 dihedral angles which is exhibited in all compounds; (4) other torsional angles (see the values of N_3P_2–N_2P_1 dihedral angles in tables 3.1 3.15) relax as well producing model compounds which are more distorted than the original lowest minimum structures. To illustrate the mode of couplings we plot two dimensional figures (3.7–3.10) of the locations of the minima as a function of the N_2P_1 N_1S_1 dihedral angle and the coupled mode. In figures (3.7) and (3.8) the coupled mode is the $S_1N_1P_1$ bond angle. In figures (3.9) and (3.10) the coupled mode is the C_2N_3-P_2N_2 dihedral angle. From these figures we note that there appears to be a one to one correspondence between the minima for the hydrogen substituted model compounds as well as for the chlorine substituted model compounds.

Figures (3.7) and (3.8) illustrate that the magnitudes of the bond angle openings are comparable in both the hydrogenated and chlorinated model compounds. In addition the scatter in the minima locations is larger in model compound with R^1=F than in model compound with R^1=Cl in the case of the hydrogen substituted. These variations are approximately comparable in the chlorine substituted model compounds. We also note that the large bond angle openings occurred in the vicinity of 240° for the N_2P_1 N_1S_1

dihedral angle in most of the model compounds.

In figures (3.9) and (3.10) the values of the C_2N_3–P_2N_2 dihedral angle range between 140° to 220°. However, these figures clearly show that there is greater scattering of points for the model compounds 1 and 2 in comparison to the model compounds 3 and 4 indicating that the dihedral angle couplings (which are not common in organic compounds) are pronounced in model compounds 1 and 2 than in model compounds 3 and 4. Which again indicate that the presence of hydrogens on phosphorus atoms makes the backbones of these model compounds less rigid. Moreover in both figures (3.9) and (3.10) when the compounds with R^1=F are compared with compounds with R^1=Cl larger variations in the minima locations are observed in compounds with R^1=F, suggesting that the compounds with fluorine on sulfur are more "flexible" than model compounds with chlorine on sulfur.

From these figures (3.7–3.10) a pattern regarding the locations of the minima can be deduced. In general one would expect that minima may be located near the following values for the N_2P_1–N_1S_1 dihedral angle: −50°, 90°, 180° and 240° for the hydrogen substituted model compounds. The corresponding values for the chlorine substituted model compounds are: −50°, 60°, 180° and 240°. Other minima may be present. For simplicity we reduced the complicated CPES to three dimensional graphs where the conformational energy differences dependence on the N_2P_1–N_1S_1 and the C_2N_3–P_2N_2 dihedral angles are shown (see figures 3.11 and 3.12). The solid bars of *o*'s or *pluses* are used as an aid in locating the minima and for the comparison of the energy differences and are thus to be taken strictly a guide to an eye.

In table (3.4) we present the energy results for the model 1 compound. The energy differences corresponding to the 0_1, 0_2 and 0_3 conformations relative to the global minimum are 1.1, 1.1, 1.4 and 2.3 kcal/mole respectively. As expected [58, 57] (from the rigid rotor and the *ab initio* calculations) these energy differences are small and fairly

flat. The actual values for the N_2P_1–N_1S_1 dihedral angle for these minima are: 93°, 242° 276° and 177°. The values of C_2N_3–P_2N_2 dihedral angles are also included in table (3.4). In table (3.8) we give similar results for the model 2 compound. The energy differences corresponding to the 0_1, 0_2 and 0_3 conformations relative to the global minimum are 0.6, 1.6, 3.0 and 3.6 kcal/mole respectively. The local minima occur at the following N_2P_1 N_1S_1 dihedral angles: 96°, −22°, 186° and 249°. The energy differences for the model compounds 1 and 2 are directly compared in figure 3.11. With the exception of the second lowest local minimum the energy differences for the model 2 compound with Cl on S_1 are somewhat higher (by approximately 1 kcal/mole) than for the model 1 compound with F on S_1. The energy differences in model 2 compound are less "flat" in comparison to the above numbers for model 1 compound. It would appear that the presence of Cl on S is energetically more costly when the full 360° rotation around the N_1 P_1 bond is performed.

In table (3.12) we present the conformational energy differences for model 3 compound. The energy differences corresponding to the 0_1, 0_2 and 0_3 conformations relative to the global minimum are 2.1, 2.4 and 4.7 kcal/mole respectively. The local minima occur at the following N_2P_1–N_1S_1 dihedral angles: 223°, 59° and 195°. These energy differences are plotted in figure 3.12.

Finally, in table (3.16) we present the conformational energy differences for model 4 compound. The energy differences corresponding to the 0_1, 0_2 and 0_3 conformations relative to the global minimum are 0.7, 2.6 and 3.3 kcal/mole respectively. The local minima occur at the following N_2P_1–N_1S_1 dihedral angles: 49°, 179° and 234°. These energy differences are also plotted in figure 3.12 and can be directly compared with the results for the model 3 compound. It is difficult to make conclusions based on these results regarding the chain flexibility. For example in model 3 compound we did not find a local minimum with as small energy difference as the one obtained for model 4 compound.

However, in both model compounds, the energy differences are comparable. We note that they are not "flat" but tend to increase as the dihedral angle, N_2P_1–N_1S_1, varies. In general the conformational energy difference in chlorine substituted model compounds are higher by 1 or 2 kcal/mole in comparison to the hydrogen substituted model compounds (although the smallest energy differences are approximately the same). In addition, it should be pointed out the order of minima located near 240° and 180° in the compound with F on S_1 is reversed in comparison to this ordering in the compound with Cl on S_1 in the hydrogen substituted model compounds. Similarly, the order of minima located near 200° and 60° in the compound with F on S_1 is reversed in comparison to this ordering in the compound with Cl on S_1 in the chlorine substituted model compounds.

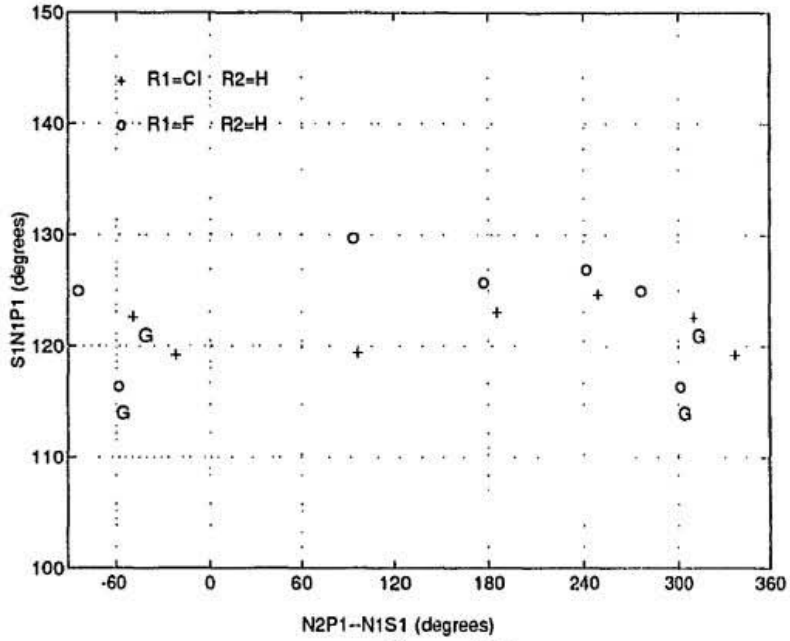

Figure 3.7

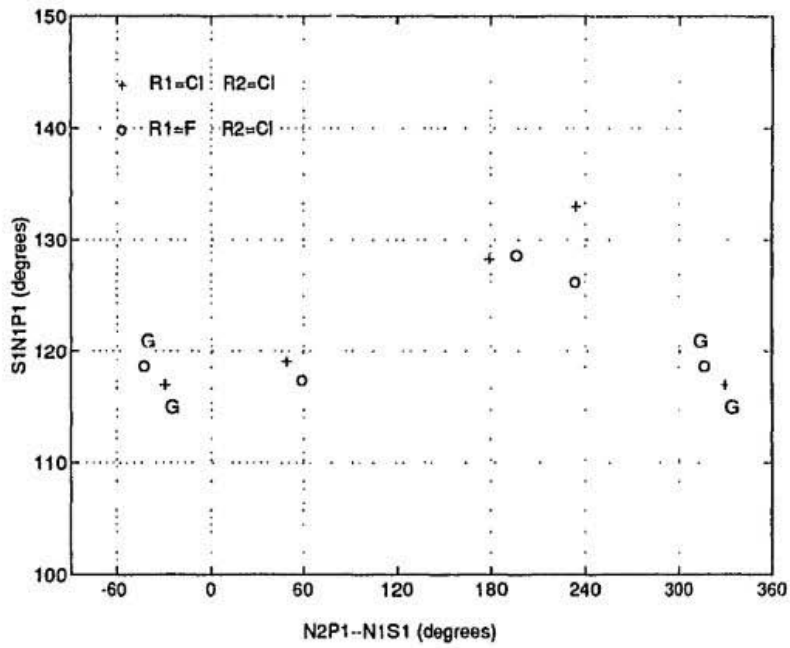

Figure 3.8

Figure 3.7: The location of the minima are shown as function of the dihedral angle N_2P_1–N_1S_1 and the bond angle $S_1N_1P_1$ (in degrees) for the model compounds 1 (R_1^1=F and R_n^2 (n=1–4) = H) and 2 (R_1^1=Cl and R_n^2 (n=1–4) = H).

Figure 3.8: The location of the minima are shown as function of the dihedral angle N_2P_1–N_1S_1 and the bond angle $S_1N_1P_1$ (in degrees) for the model compounds 3 (R_1^1=F and R_n^2 (n=1–4) =Cl) and 4 (R_1^1=Cl and R_n^2 (n=1–4) =Cl). The capital letters, Gs, indicate the location of the global minima.

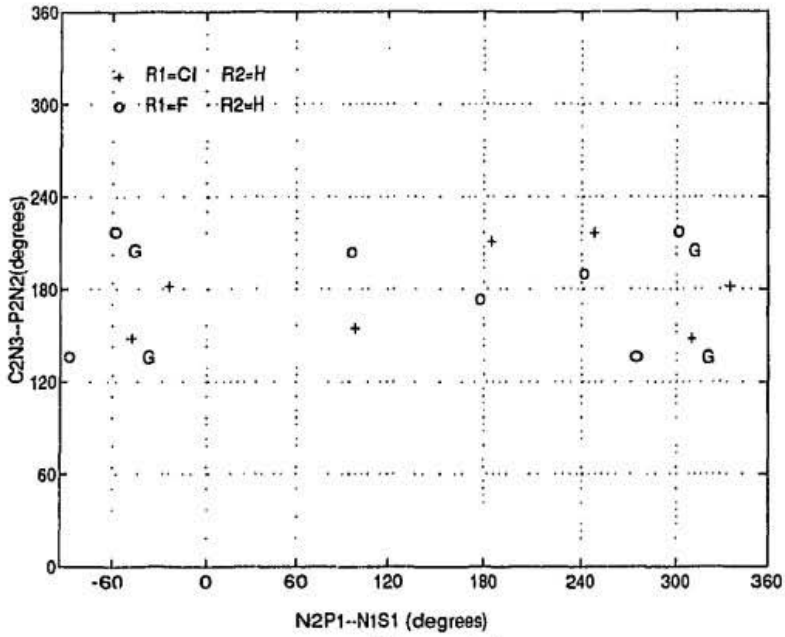

Figure 3.9

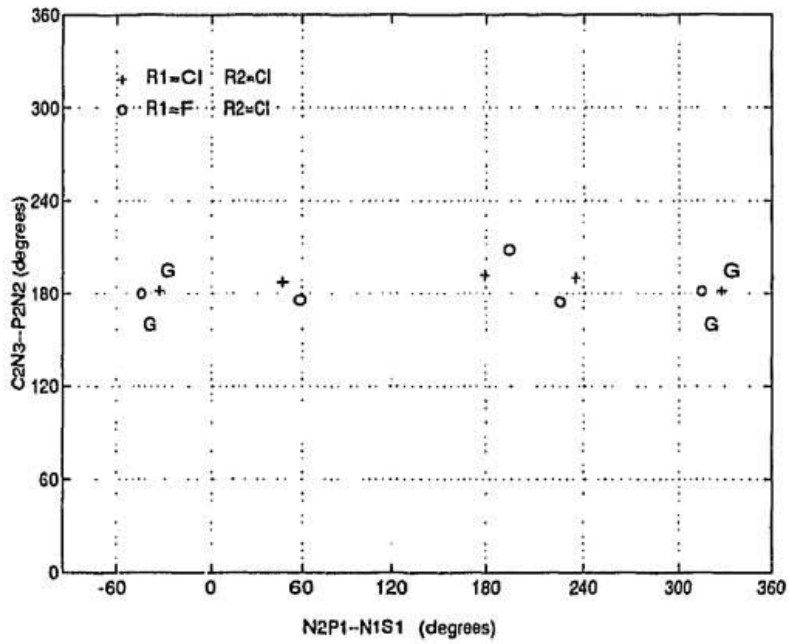

Figure 3.10

Figure 3.9: The location of the minima are shown as a function of two dihedral angles N_2P_1–N_1S_1 and C_2N_3–P_2N_2 (in degrees) for the model compounds 1 (R_1^1=F and R_n^2 (n=1-4) =H) and 2 (R_1^1=Cl and R_n^2 (n=1-4) =H).

Figure 3.10: The location of the minima are shown as function of two dihedral angles N_2P_1–N_1S_1 and C_2N_3–P_2N_2 (in degrees) for the model compounds 3 (R_1^1=F and R_n^2 (n=1-4) = Cl) and 4 (R_1^1=Cl and R_n^2 (n=1-4) =Cl). The capital letters, Gs, indicate the location of the global minima.

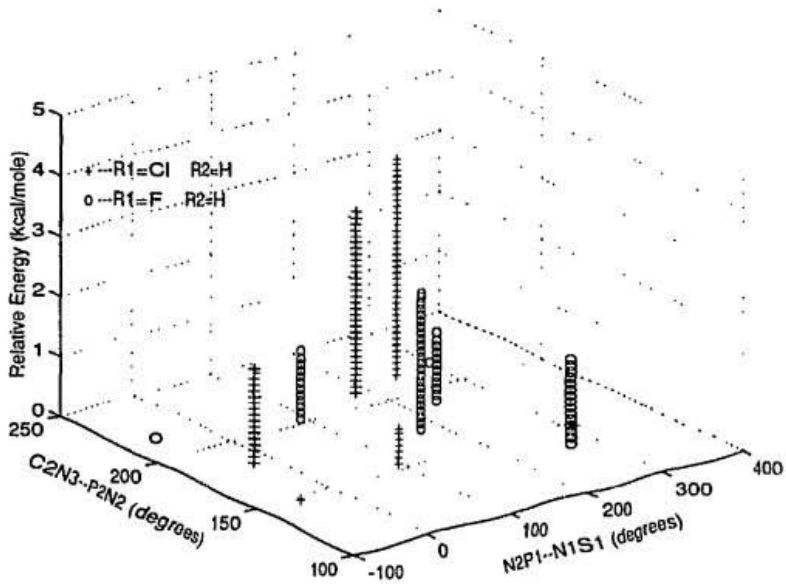

Figure 3.11

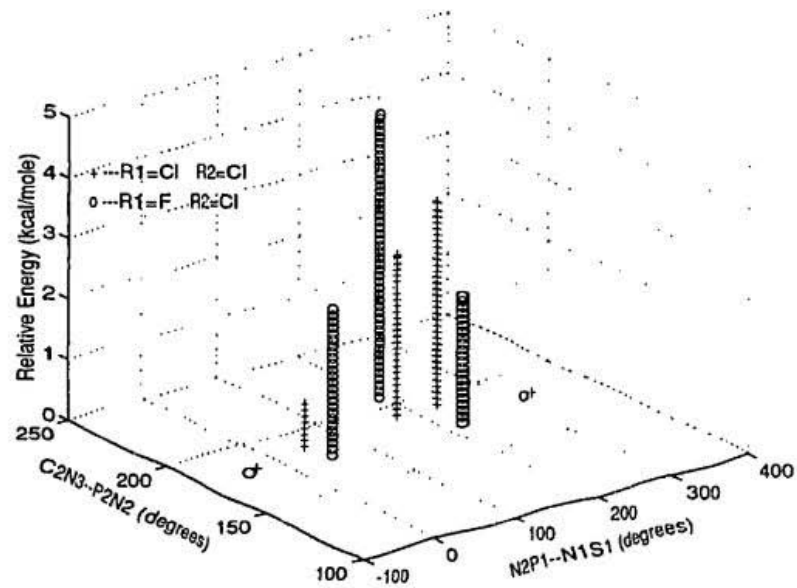

Figure 3.12

Figure 3.11: The variation of the conformational energy differences (in kcal/mole) is shown as a function of two dihedral angles N_2P_1- N_1S_1 and C_2N_3 P_2N_2 (in degrees) for the model compounds 1 (R_1^1=F and R_n^2 =H) and 2 (R_1^1=Cl and R_n^2 =H) (n=1 4).

Figure 3.12: The variation of the conformational energy differences (in kcal/mole) is shown as a function of two dihedral angles N_2P_1-N_1S_1 and C_2N_3-P_2N_2 (in degrees) for the model compounds 3 (R_1^1=F and R_n^2 = Cl) and 4 (R_1^1=Cl and R_n^2 = Cl) (n=1 4).

Chapter 4

Classical Poly(phosphazenes)

In this chapter we will present the results of our DFT calculations for the inorganic polymers classical poly(phosphazenes) (CPPs) (see figure 1.2). The polymer backbone consists of alternating phosphorus and nitrogen atoms, with two side groups, R, attached to each phosphorus. We investigated the global and local minima of CPPs with only one type of substituent (R=Cl). We label this model compound as model 7 with R=Cl.
The rotation around N_1–P_2 bond (same as N_1–P_1 bond in model compounds 1-4, but the atom numbering will be different.) is indicated as ϕ in figure 4.1. The completely optimized geometrical parameters (that is bond lengths, bond angles and dihedral angles), the energies and the corresponding energy differences between the global and the local minima conformations are given in tables (4.1-4.4) The torsional angles ϕ's are given as N_2P_2 N_1P_1 dihedral angles. We are using the same type of notations 0_0 and 0_n (n=1,2..) for global and local minima structures as in the previous chapter (3). The geometry optimized, near planar, trans-cis, global minimum structure for the model 7 compound

is displayed in the figure 4.1.

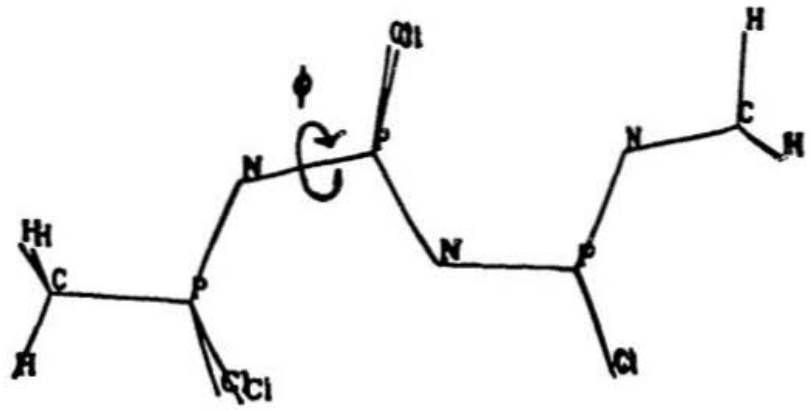

Figure 4.1: Stick figure of model 7 compound (R=Cl) with the plane formed by P-N-P atoms parallel to the paper. The geometries plotted correspond to the global minimum parameters given in tables (4.1—4.4).

4.1 Structural Analysis

CPPs with only one type of side group exhibit more symmetry and regularity than PTPs. For the model 7 compound we have found four local minima in addition to the global one and the global minimum assumes a planar cis-trans conformation. The corresponding model compound in PTPs is the model 4 compound.

In agreement with the experimental studies [17], the bonding structure in the backbone of all conformations is represented as a series of alternating single and double bonds. It can be seen that, all single N-P bonds are nearly the same length within the conformation and between the other conformations. Similarly the double bonds $P_1=N_1$ and $P_2=N_2$ have nearly the same length in all conformations. The bond length $P_3=N_3$, is shorter than the "double" bond, P=N, in all conformations. This shorter bond length is also seen in model 4 compound ($P_2=N_3$) and in model 6 compound ($P_2=N_3$). In all local

minima conformations (0_1 to 0_3) we can see small decrease in the P–N bonds (single and double) in the first half of the model compound and small increase in the P–N bonds (single and double) in the second half of the chain in comparison to the global minimum 0_0. The difference between single and double bonds ($\approx 0.07\mathring{A}$) is not as large as in the PTPs ($0.1\mathring{A}$). In contrast to the PTPs, all P–R bonds have the same bond lengths in all conformations. Overall the bond lengths show no substantial variations between the conformations or within the conformation. Thus, the bond lengths are relatively unaffected by the conformational changes. (see table 4.1)

In this model compound, similar to PTPs model compounds, we observe $P_1N_1P_2$ bond angle opening. The $P_1N_1P_2$ bond angle opens up 2°, 11° and 13° in the second, third and fourth local minima respectively. Small decrease (5°) has been observed in the 0_2 conformation, this decrease is accompanied by an opening of $P_1N_2P_3$ bond angle by 5° relative to the 0_0 conformation. Another important observation is that, in all conformations the angles, $R_1P_1N_1$ and $R_2P_1N_1$, are much bigger than the remaining RPN bond angles which are close to 105°. The difference is $\approx$11°. This is true in all conformations. This may be attributed the end group effect. All the other bond angles remain relatively insensitive to the rotations. There is some variation in the $P_2N_2P_3$ with some decrease or some increase by a few degrees depending on the conformation. (see table 4.2)

From dihedral angle values (see table 4.3) we note that the rotation around the N_1–P_2 bond is coupled to other rotational mode, that is P_3–N_2 bond is also simultaneously rotated, as exhibited by the values of N_3P_3–N_2P_2 dihedral angles. These couplings are not the same type that have been observed in PTPs. Deviations of the dihedral angle N_3P_3 N_2P_2 in local minima 0_1, 0_2, 0_3 and 0_4, from that of global minimum 0_0 are 15°, 36°, 13.5° and 2.5°. The dihedral angles P_3N_2–P_2N_1 and C_2N_3–P_3N_2 in the first local minimum deviated from their expected values 180° by 15°, where as they are almost

180° in all global and local minima conformations. The position of the substituent R_1 relative to the backbone is readjusted by 10° to 15° depending on the conformation. This could compensate for the increase in the bond angle $R_1P_1N_1$. The important conclusion regarding the dihedral angles is that, the rotation around $N_1 \cdot P_2$ bond affected the neighboring dihedral angles. This suggests that the distortions due to the rotation are more localized.

Table 4.1: Comparison of bond lengths (Å) for the global (0_0) and the local minima (0_k,k=1 3) of CPPs with R=Cl.

Bond	0_0	0_1	0_2	0_3	0_4
$P_1=N_1$	1.570	1.579	1.568	1.557	1.556
N_1-P_2	1.627	1.633	1.626	1.621	1.621
$P_2=N_2$	1.571	1.571	1.569	1.564	1.560
N_2-P_3	1.632	1.629	1.634	1.633	1.630
$P_3=N_3$	1.541	1.538	1.539	1.542	1.541
P_1-R_1	2.033	2.039	2.033	2.041	2.041
P_1-R_2	2.034	2.029	2.034	2.039	2.041
P_2-R_3	2.032	2.036	2.037	2.053	2.046
P_2-R_4	2.030	2.034	2.028	2.042	2.047
P_3-R_5	2.087	2.094	2.074	2.078	2.083
P_3-R_6	2.082	2.081	2.100	2.085	2.084
N_3-C_2	1.438	1.439	1.440	1.437	1.437
C_1-P_1	1.783	1.779	1.783	1.781	1.783
C_1-H_1	1.103	1.103	1.103	1.102	1.103
C_1-H_2	1.104	1.104	1.105	1.104	1.105
C_1-H_3	1.104	1.105	1.104	1.104	1.105
C_2-H_4	1.111	1.109	1.110	1.110	1.109
C_2-H_5	1.106	1.107	1.107	1.106	1.105
C_2-H_6	1.111	1.112	1.111	1.111	1.111

Table 4.2: Comparison of bond angles (degrees) for the global (0_0) and the local minima (0_k,k=1-3) of CPPs with R=Cl.

Bond angle	0_0	0_1	0_2	0_3	0_4
$\angle R_1P_1N_1$	115.990	116.931	116.150	116.141	115.621
$\angle P_1N_1P_2$	123.728	119.059	125.494	134.653	137.413
$\angle N_1P_2N_2$	110.650	109.603	111.747	109.002	109.094
$\angle P_2N_2P_3$	123.596	128.103	124.868	121.076	123.465
$\angle N_2P_3N_3$	113.303	114.408	114.557	113.244	113.895
$\angle R_2P_1N_1$	116.308	115.942	116.078	115.268	115.953
$\angle C_1P_1N_1$	108.929	109.565	109.171	110.528	110.873
$\angle R_3P_2N_1$	105.136	105.428	105.446	107.806	106.636
$\angle R_4P_2N_1$	104.950	106.316	104.658	105.437	107.004
$\angle R_5P_3N_2$	103.904	104.226	102.855	103.344	104.181
$\angle R_6P_3N_2$	104.127	103.399	104.154	105.300	103.590
$\angle H_1C_1P_1$	110.675	109.951	110.533	110.242	109.861
$\angle H_2C_1P_1$	107.964	108.259	108.056	108.149	107.877
$\angle H_3C_1P_1$	107.883	108.927	107.943	107.986	108.590
$\angle C_2N_3P_3$	128.011	127.813	128.262	127.606	129.206
$\angle H_4C_2N_3$	112.638	113.176	112.257	112.432	112.800
$\angle H_5C_2N_3$	108.798	108.763	108.908	108.697	108.664
$\angle H_6C_2N_3$	112.487	112.190	113.014	112.585	112.663

Table 4.3: Comparison of dihedral angles (Å) for the global (0_0) and the local minima (0_k,k=1-3) of CPPs with R=Cl.

Dihedral angle	0_0	0_1	0_2	0_3	0_4
$\angle P_2N_1$-P_1R_1	-63.501	-66.139	-62.718	-49.117	-62.187
$\angle N_2P_2$-N_1P_1	0.516	7.546	-7.195	-162.846	177.464
$\angle P_3N_2$-P_2N_1	-178.139	-156.148	179.475	178.644	-177.244
$\angle N_3P_3$-N_2P_2	-0.964	-15.346	34.699	12.505	1.451
$\angle R_1P_1$-N_1R_2	122.201	122.110	121.516	120.701	121.124
$\angle C_1P_1$-N_1R_1	118.927	120.129	119.631	119.249	119.752
$\angle R_3P_2$-N_1N_2	125.893	124.680	124.471	126.249	125.124
$\angle R_4P_2$-N_1R_1	107.890	107.677	108.618	108.481	108.667
$\angle R_5P_3$-N_2N_3	128.088	127.662	128.347	128.106	128.078
$\angle R_6P_3$-N_2R_3	103.341	102.110	103.384	103.677	103.312
$\angle H_1C_1$-P_1R_1	54.409	55.511	53.481	56.55	51.966
$\angle H_2C_1$-P_1H_1	-120.760	-120.110	-120.658	-121.077	-120.574
$\angle H_3C_1$-P_1H_1	120.739	120.894	120.700	120.346	120.749
$\angle C_2N_3$-P_3N_2	-179.892	162.710	174.961	-175.555	174.287
$\angle H_4C_2$-N_3P_3	59.200	67.591	76.434	54.634	65.564
$\angle H_5C_2$-N_3H_4	119.052	119.436	118.687	119.083	119.057
$\angle H_6C_2$-N_3H_4	-122.029	-122.230	-122.210	-122.066	-122.082

Table 4.4: Comparison of total energies (hartrees) and corresponding energy differences (given in hartrees and kcal/mole) for the global (0_0) and the local minima (0_k,k=1-3) of CPPs with R=Cl.

minimum	E_{total}(har)	$\angle N_2P_2$-N_1P_1	ΔE(har)	ΔE(kcal/mole)
0_0	-4014.605993	0.516	—	—
0_1	-4014.605463	7.546	0.0005	0.33
0_2	-4014.605458	-7.195	0.0005	0.33
0_3	-4014.605093	-162.846	0.0009	0.56
0_4	-4014.604220	177.46	0.0018	1.10

4.2 Conformational Analysis

In this section we examine the locations and the energies of the local minima relative to the global minimum in the CPPs model compounds. The global minimum of the model compound has a planar cis-trans conformation. The conformations assumed by the model compound can be understood mainly in terms of the repulsions or attractions between the side groups attached to nearby phosphorus atoms. The cis-trans planar conformation allows the side groups to move as far away from each other as possible. Hence, this conformation should minimize the repulsions and generate the lowest energy. Our DFT calculations tend to confirm this supposition for all model compounds. The expected symmetry and the regularity of the model compound is not disturbed.

In the previous section we have discussed the structural changes between conformations. Similar to PTPs, we observe bond angle openings and dihedral angle couplings in CPP model compound, although the couplings are not necessarily of the same type.

From these figure (4.2) a pattern regarding the locations of the minima can be deduced. In general one would expect that minima may be located near the following values for the N_2P_2–N_1P_1 dihedral angle for CPPs: 0°, 90°, 180°, and 240°. But, surprisingly we could not find any minima near 90°. The global and local minima occur at the following N_2P_2–N_1P_1 dihedral angles: 0°, 8°, -7°, −163°, and 177°.

In table (4.4) we present the conformational energy differences for the model 7 compound. The actual values of N_2P_2–N_1P_1 dihedral angles are also included in table (4.4). The energy differences corresponding to the 0_1, 0_2, 0_3 and 0_4 conformations relative to the global minimum are 0.33, 0.33, 0.56, and 1.10 kcal/mole respectively. These energy differences are plotted in figure 4.3, as a function of angle of rotation. As expected the energy differences in this model compound are significantly smaller than the energy differences for the other model compounds studied so far. These small energy differences (at

a given temperature) suggest that CPP model compound is more "flexible" than PTP model compounds.

4.3 Comparison between CPP and PTP.

In this section we will discuss about the structural differences between the conformations of the CPPs and PTPs with chlorine substituents on phosphorous atoms. In order to see how the presence of sulfur in backbone chain of the PTPs affects the conformational stability, we compare the optimized geometrical parameters of the CPP model compound (7), with the ones in PTP model compounds (4, 6).

The optimized geometrical parameters (bond lengths, bond angles and dihedral angles) for PTP and CPP model compounds are given in tables (3.13–3.16, 4.1–4.4). In the global minimum conformations, it can be seen that there are no significant variations in the bond lengths except slight changes in the P–N bond lengths near sulfur (see tables 3.13, 4.1). Similarly there are no big differences in the bond angles. But PNP bond angle is decreased by 4° whereas NPN bond angles along the backbone are not affected by the presence of sulfur.

Significant differences are observed in the dihedral angles. We can see that, (see tables 3.15, 4.3) the presence of sulfur caused rotation ($\approx 30°$) around N_1-P_2 bond and distorts the planarity (cis) near sulfur, as exhibited by the values of $N_2P_2-N_1P_1$ and $N_2P_1-N_1S_1$ dihedral angles. This dihedral angle $N_2P_1-N_1S_1$ deviated almost 30° from the cis conformation. This trend is not true for all dihedral angles along the backbone. In PTPs other dihedral angles along the backbone $P_2N_2-P_1N_1$, $N_3P_2-N_1P_1$ and $C_2N_3-P_2N_2$ indicate that the chain backbone has acquired a planar structure except near the sulfur atom. In PTPs only one dihedral angle near sulfur deviated from the planar structure by large amount, with the remaining dihedral angles close to the ideal values whereas

CPPs have complete planar structure. This trend is completely reversed in the local minima conformations of PTPs (see tables 3.13. All local minima of CPPs are very close to planar structure, whereas all local minima of PTPs are distorted a lot from planarity (not only near sulfur).

The energy differences between different conformations of CPPs are smaller than the corresponding values in PTPs (see tables (4.4), (3.12)). The full rotation around the N_1-P_2 bond in CPPs is inexpensive energetically. Our computations also show that, the calculation of the local minima in CPPs were relatively straight forward in comparison to PTPs. Based on the energy differences we can say that the CPP backbone is more flexible than the backbone of PTPs. So, the presence of the highly polar S=O group tends to decrease skeletal flexibility relative to CPPs.

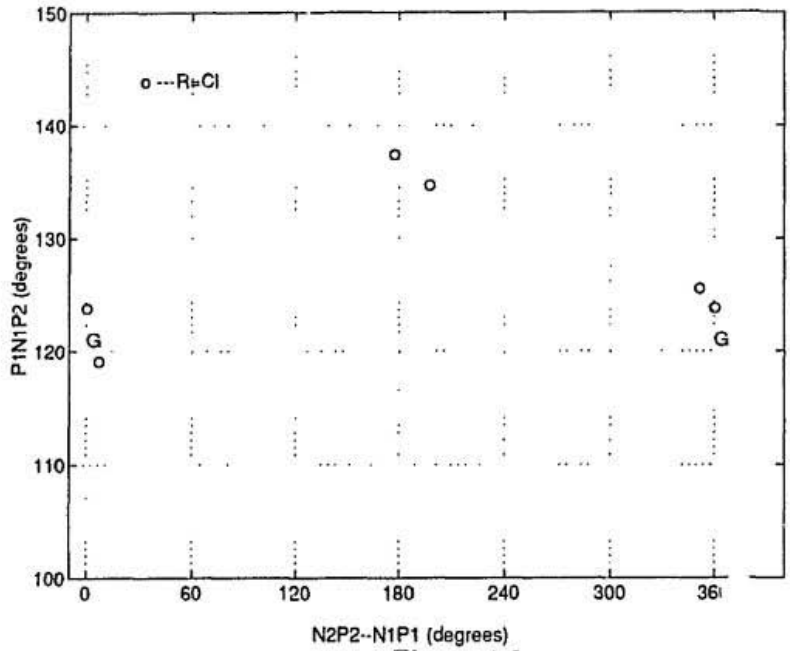

Figure 4.2

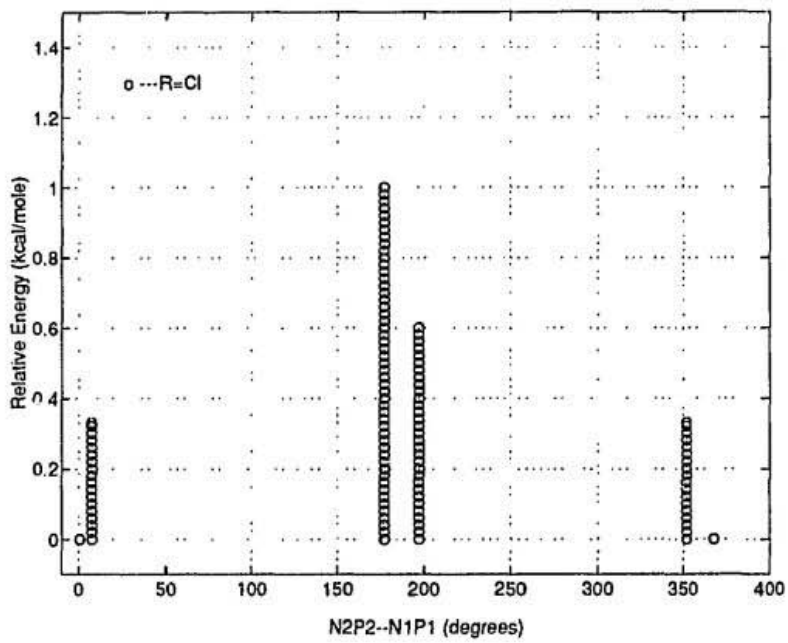

Figure 4.3

Figure 4.2: The location of the minima are shown as function of the dihedral angle N_2P_2 N_1P_1 and the bond angle $P_1N_1P_2$ (in degrees) for the model compound 7 (R=Cl). The capital letters, Gs, indicate the location of the global minima.

Figure 4.3: The variation of the conformational energy differences (in kcal/mole) is shown as a function of dihedral angle N_2P_2–N_1P_1 (in degrees) for the model compounds 7, (R=Cl).

Chapter 5

Radial density distribution - Charge delocalization

The skeletal bonds in phosphazenes are not like their counterparts in classical organic polymers. To understand the differences, it is necessary to consider the dispositions of the valence electrons in a short segment of the chain. Each phosphorus atom provides five valence electrons per repeating unit, and each nitrogen contributes an additional five. If two of the electrons from nitrogen are confined to a lone pair orbital, and electron pairs are assigned to the sigma bond framework, two electrons are left unaccounted for; one from phosphorus and one from nitrogen. These electrons do not remain unpaired. It is believed that the electron on nitrogen is accommodated in a $2p_z$ orbital, and the one from phosphorus in a $3d$ orbital. It is believed that the pi-bonds are delocalized over three atoms [59]. They are not broadly delocalized over the whole chain because of the orbital mismatch and nodes that occur at every phosphorus and sulfur in PTPs. The charge transfer and the electronic structure of these compounds have not yet been studied in detail at a quantum mechanical level.

We have plotted, (see figure, 5.1) the main result of the calculation $4\pi r^2\rho(r)$ as the appropriate measure of the magnitude of the radial charge density [60] at distance r from the nucleus. The radial density distribution function is computed from the spherically averaged numerical density. Here $\rho(r)$ denotes the spherical average of electronic charge density $\rho(\mathbf{r})$. The radial charge density ($4\pi r^2\rho(r)$) is the amount of charge contained between r and r+dr.

The electron density distribution of the atoms (along the backbone), corresponding

to the equilibrium geometries, (for PTPs and CPPs) have been plotted in figure (5.1). In each plot we have one backbone atom and its neighboring atoms along the backbone. We plot the electron density distributions of one main atom and its mirror image and the two neighbor atoms, whereas the main atom is taken as the reference of scale. We plotted this way because the pi-bonds are delocalized over three atoms, and it is easier to see the charge delocalization in both directions. All atoms are separated by the interatomic distances, obtained from our calculations.

Also in figures (5.2) we have plotted the electronic configurations of the free atoms P, N, S etc., Consideration of these atoms will help us in the analysis of charge transfer effects. To be more precise, we have calculated the electron density distribution of the isolated atoms. We define the densities of isolated atoms as "atomic densities" and the densities of atoms from the model compound as "molecular densities". The atomic densities are represented by the dotted curves in figures (5.2). In all density distributions the inner part of the curve corresponds to bound state (core electron) density distribution and the outer part of the curve corresponds to the valence density distribution. Comparing the atomic densities with the molecular densities, we can observe that in the molecular densities (for phosphorus atom, sulfur atom) a depletion of the electronic density in the outer part of the curve (which corresponds to the contribution from the valence electrons) and an accumulation of extra charge (for nitrogen atoms) in the similar region, which indicates the charge transfer towards N from P.

The transfer of charge from the phosphorus and sulfur atoms towards nitrogen is clearly seen in figures (5.3), where we have plotted

$$\Delta\rho(r) = \rho(r) - \rho_{at}(r) \tag{5.1}$$

where $\rho(\mathbf{r})$ is the density of the atoms of our model compounds, and $\rho_{at}(r)$ is the density of the "isolated" atoms. $\Delta\rho$ is negative in the outermost part of the curve for phosphorus

and sulfur atoms and it is positive for nitrogen atoms. What is apparent from these figures is that the core electron density is almost exactly the same for both isolated and bonded (atoms from the model compounds) atoms. Only in the valence region, there is a significant difference. A reasonable quantitative measure of the charge transfer ΔQ can be given by;

$$\Delta Q = \int (\rho(r) - \rho_{at}(r))dr. \tag{5.2}$$

This gives the values of '-0.875' , '$+0.51$' and '-0.91' for the charge transfer in P, N and S respectively. The charge transfer from P to N or S to N are not exactly equal to the charge accumulation on N, because some charge is transferred to the other backbone elements and the substituents, which we have not shown. The other region of oscillatory values of $\Delta\rho$, between 0 and 2 au, illustrates that even though the "core" electron densities are not affected very much when atoms are covalently bonded, however small, measurable charge redistributions occur near the nucleus as well.

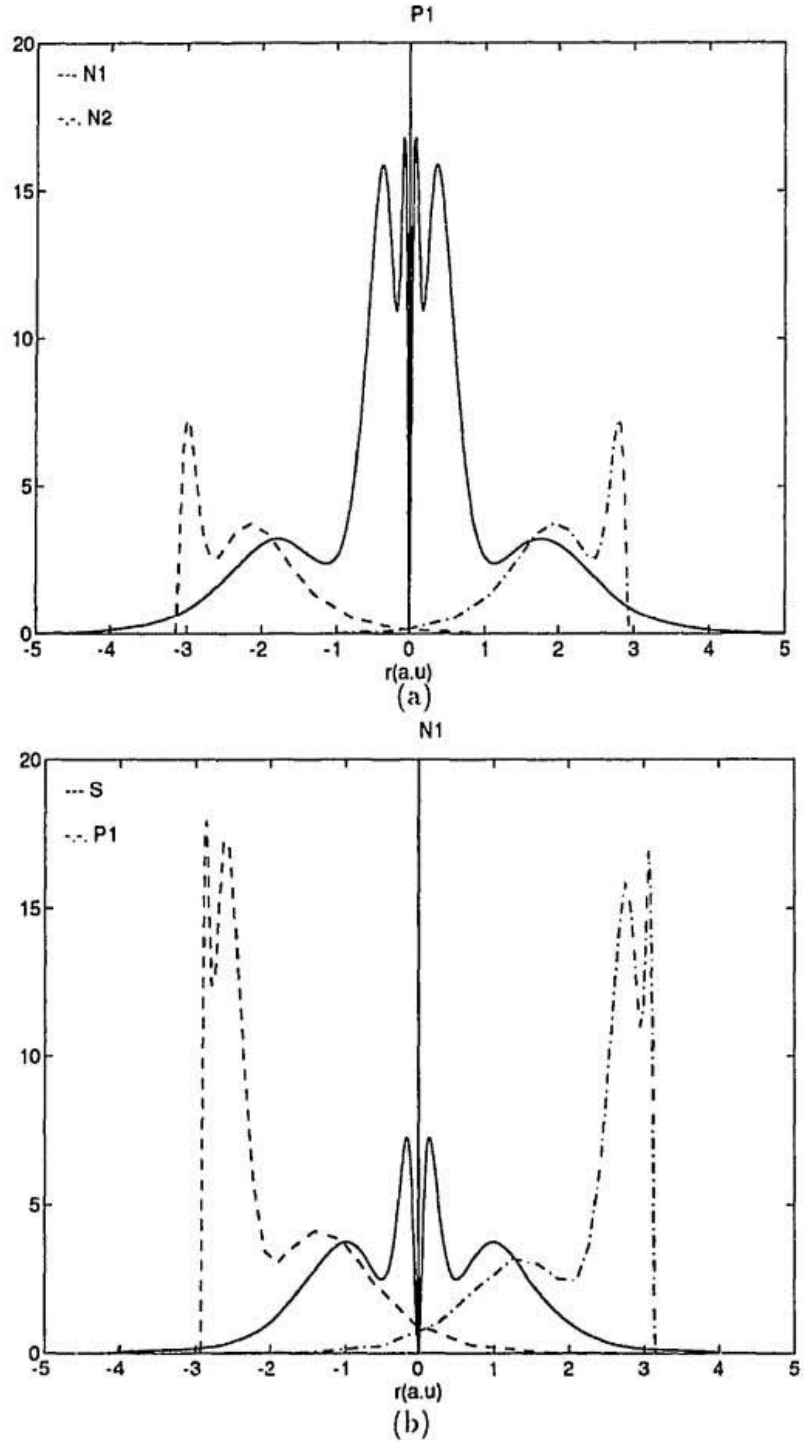

Figure 5.1: Plots of the radial charge density distributions $4\pi r^2\rho(r)$ as a function of radial atomic distances r (a.u) for the atoms along the backbone, (a) Phosphorus (b) Nitrogen (c) Sulfur.

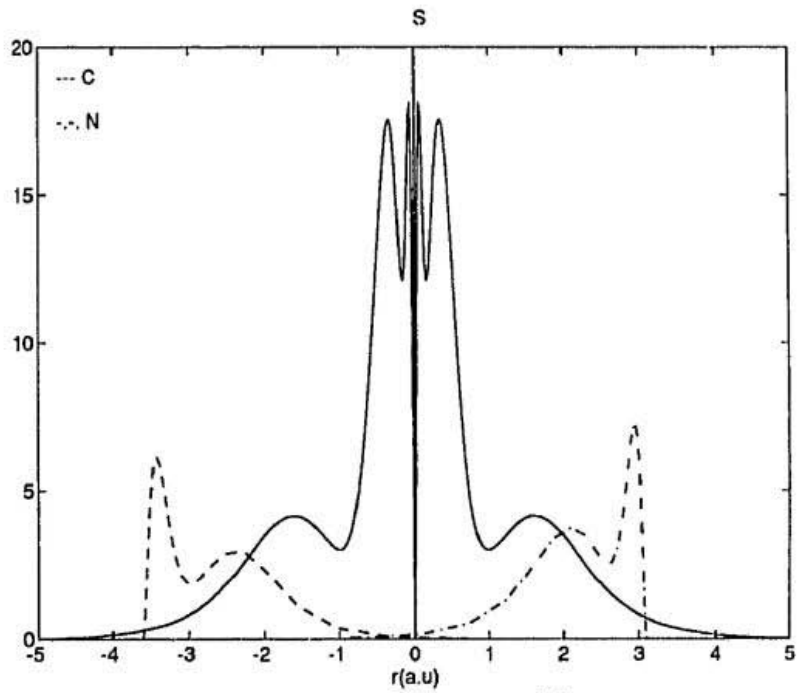

Figure 5.1 (c)

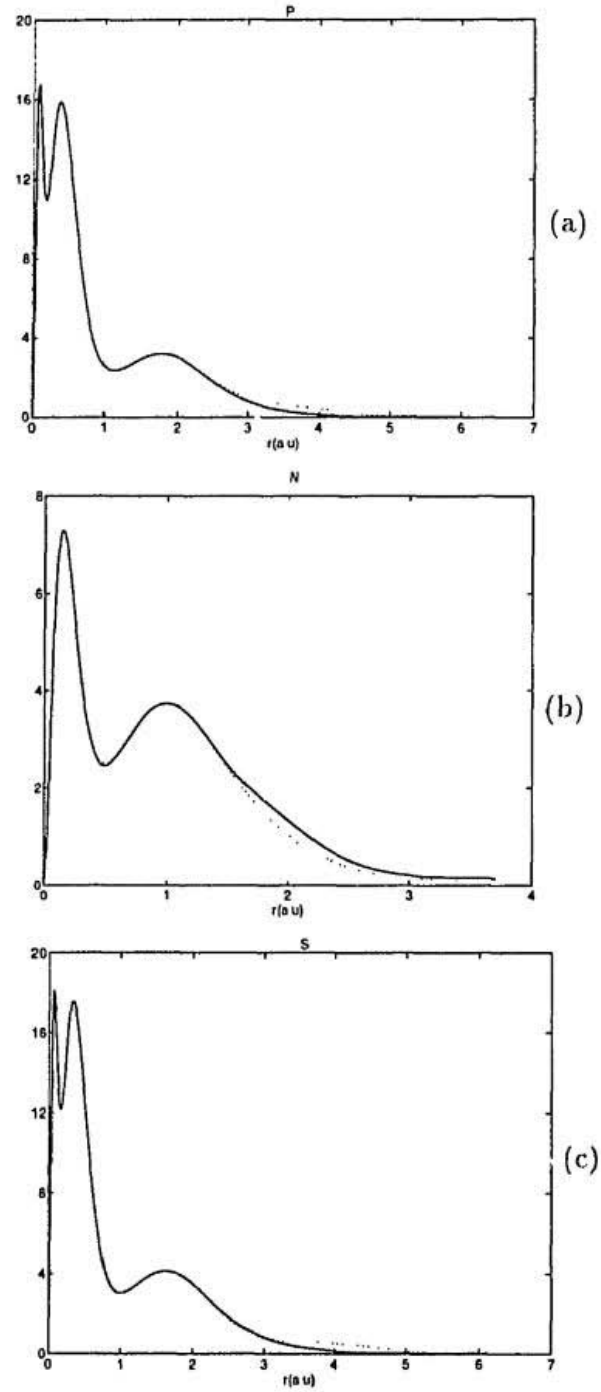

Figure 5.2: Plots of the radial charge density distributions $4\pi r^2\rho(r)$ as a function of radial atomic distances r (a.u) for the model compound atoms (solid line) and isolated atoms (dotted line) along the backbone, (a) Phosphorus (b) Nitrogen (c) Sulfur.

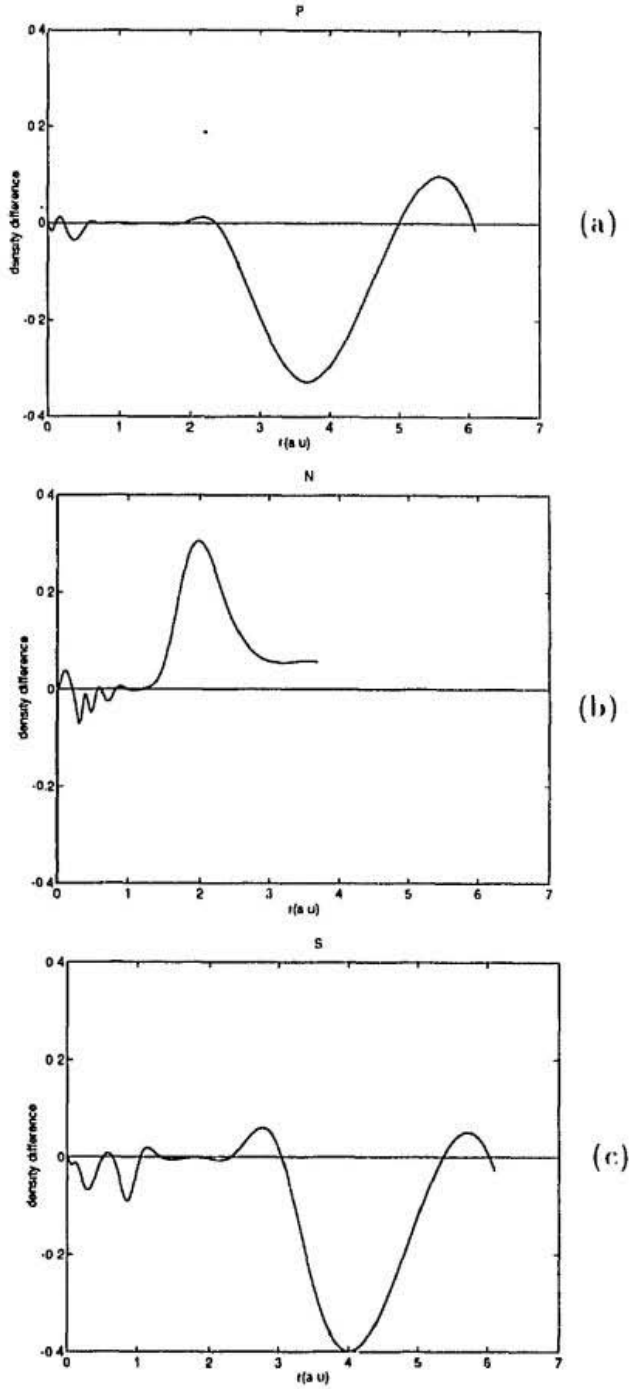

Figure 5.3: Plots of the radial charge density difference $4\pi r^2(\rho(r) - \rho_{at}(r))$ between the "molecular" densities and "atomic" densities as a function of radial atomic distances r (a.u) for the atoms along the backbone, (a) Phosphorus (b) Nitrogen (c) Sulfur.

Chapter 6

Relationship between the conformational analysis (chain flexibility) and glass transition behaviour.

In this section we will discuss the relationship between the conformational analysis and the glass transition temperature. Polymer flexibility is often defined in terms of the glass transition temperature T_g [61]. Inorganic polymer chains which generally exhibit high flexibility have relatively low glass transition temperatures. A polymer with high T_g is believed to have a backbone that offers more resistance to bond torsion than a polymer with a low T_g. The glass transition temperature is of considerable practical, as well as fundamental importance.

Poly(phosphazenes) are said to be very flexible macromolecules. Several structural features make the poly(phosphazenes) (including PTPs) backbones very flexible in all of polymer science. The reasons for the extraordinary flexibility can be seen from the structural parameters of the compounds (see tables 3.5 to 4.3). First, because of the nature of the bonding, [62] the P−N and P=N skeletal bonds have lengths (1.64$\mathring{A}$, 1.57$\mathring{A}$) which are larger than that (1.53 $\mathring{A}$) of the C−C bond found in most organic polymers. As a result, steric interferences or intramolecular interactions are diminished. But, in PTPs one of the skeletal bonds, S=N has a length (1.525$\mathring{A}$) which is shorter than that of the C−C bond. This could be one of the reasons for decrease in the chain flexibility of PTPs compared to CPPs. Also, the nitrogen skeletal atoms are small but still have the trivalency needed to continue a chain structure, and also the side groups are not affected by the nitrogens. Finally the PNP bond angle ($\sim 125°$) is more open

than the usual tetrahedral bonding (~110°), and torsional rotations can occur without incurring a serious energy penalty. (The corresponding S -N P bond angle (117°) is always smaller than the P—N—P bond angle in PTPs). These structural features have the effect of increasing the flexibility of the chain.

In tables 6.1, 6.2 and 6.3 we summarise the conformational analysis discussed in previous chapters and relate it to the glass transition temperatures of the corresponding compounds. From the tables it is seen that the PTPs have very flexible backbones (their conformational energy differences are smaller than the conformational energy differences for the rotation around single C—C bond in organic compounds, see for example [63]). Our calculations show that the energy differences between conformations are of the order of less than 1 kcal/mole to 5 kcal/mole. The height of the rotation barriers was estimated from the rigid rotor calculations and it was found that the height of the barriers were in the 5–10 kcal/mole [58]. By combining all these results we note that the chain backbones of the PTP model compounds with F and Cl on sulfur are flexible, however the expected correlation of the energy differences with the T_gs (lower T_gs corresponding to lower energy differences) has not been observed. Conformational energy differences for CPP model compounds are very small, (see table 6.3) when compared to the conformational energy differences for the rotation around single P—N bond in PTP model compounds. Our calculations show that these energy differences for CPP model compounds are of the order of less than 1 kcal/mole. They have the smallest values among all energy differences for the model compounds we have studied. In addition we note that when the structures (global minima) of the CPP and PTP model compounds are compared, all bond lengths and bond angles along the chain backbone are longer for CPP model compound. These are clear evidences for the high flexibility of the chain, which in this case can be correlated with the lower T_g for the CPP systems.

Table 6.1: Energy differences between different conformations and the glass transition temperature of PTPs with R^1=F and R^2_n=Cl, (n=1–4)

minimum	ΔE(har)	ΔE(kcal/mole)	T_g
0_1	0.0033	2.1	
0_2	0.0038	2.4	-56°
0_3	0.0074	4.7	

Table 6.2: Energy differences between different conformations and the glass transition temperature of PTPs with R^1=Cl and R^2_n=Cl, (n=1–4)

minimum	ΔE(har)	ΔE(kcal/mole)	T_g
0_1	0.0011	0.7	
0_2	0.0042	2.6	-46°
0_3	0.0053	3.3	

Table 6.3: Energy differences between different conformations and the glass transition temperature of CPPs with R=Cl.

minimum	ΔE(har)	ΔE(kcal/mole)	T_g
0_1	0.00003	0.02	
0_2	0.00053	0.33	
0_3	0.00090	0.56	-63°
0_4	0.00177	1.10	

Chapter 7

Conclusions

The discussion of the structural and conformational analyses indicate that the rotation around N_1–P_1 bond in PTP model compounds leads to significant relaxations of the other geometrical parameters. Some variations in the bond lengths have been observed. Also, the SNP bond angle openings as well as coupling between the N_2P_1 N_1S_1 and C_2N_3–P_2N_2 dihedral angles are present. These couplings are shown in figures (3.9) and (3.10). In general one expects that in these model compounds the minima on the CPES may be located near the following values of the N_2P_1–N_1S_1 dihedral angle: $-50°$, $90°$ (or $60°$), $180°$ and $240°$. The values of the conformational energy differences are between 0.6 and 5 kcal/mole. From the above discussion we also find that the energy differences for the monomers with fluorine on the sulfur are smaller than the corresponding energy differences for the monomers with chlorine on the sulfur in the hydrogen substituted compounds. This is not the case in the chlorine substituted compounds which indicates that energies are comparable. The structural analysis indicates that the compounds with fluorine on the sulfur exhibit more distortions (changes in bond lengths, bond angles and dihedral angles due to the rotation) along the backbone than compounds with chlorine on the sulfur. This could account for the lower T_g for these compounds.

In CPPs structural and conformational analyses indicate that the rotation around N_1 P_2 bond leads to some relaxations of the other geometrical parameters. Symmetry and regularity has been observed in all conformations. PNP bond angle openings are present. The rotation around N_1–P_2 bond is coupled with other rotational modes, although not

the same as in PTPs. The distortion caused by the rotation has only local effect. For CPP model compounds we found minima near the following values of $N_2P_2-N_1P_1$ dihedral angle: 0°, 8°, −7°, −163° and 177°. The conformational energy differences for these compounds are very small (less than 1 kcal/mole), which indicate that full rotation (360°) around N_1-P_2 bond is energetically inexpensive. The structural analysis and the conformational energy differences indicate, that CPPs backbone is more flexible than the backbone of PTPs. The presence of sulfur leads to a decrease in skeletal flexibility.

The radial charge density distribution function, $D(r)=4\pi r^2\rho(r)$ is computed from the spherically averaged numerical densities. The charge distribution along the backbone chain is explained. Using the spherically averaged total electron densities it is shown that the charge along the backbones of the model compounds is partially delocalized and accumulates primarily on the nitrogen atoms. Mulliken population analysis [64] from our calculations is also suggesting the same.

Finally, we correlated the conformational analysis results with the experimentally obtained, T_gs. The results are in good agreement for hydrogenated PTPs and CPPs.

Acknowledgments

I would like to offer my sincere thanks to Dr. Jolanta Lagowski, without whom this thesis would not be. Her teaching, patience, enthusiasm and valuable advises made this work more enjoyable and of much higher quality than would have been the case without her participation.

I would like to thank the High Performance Computing Center in Calgary, Alberta for the support with some of our computations. With regard to which I would like to thank Dr. A.J. Stacey for helping us with the code compilation on the Fujitsu Supercomputer.

I would like to thank Dr. D. R. Salahub, Department of Chemistry at the University of Montreal, for allowing us to use *deMon* program.

I would like to offer special thanks to Dr. Raymond A. Poirier, Dr. M. R. Morrow and Dr. J. R. de Bruyn for their reading of my thesis, constructive criticism and helpful suggestions.

For financial support I would like to thank the Natural Sciences and Engineering Research Council of Canada (NSERC) and Memorial University of Newfoundland for their generous support.

Bibliography

[1] J.E. Mark, H.R. Allcock, and R. West. *Inorganic Polymers, Prentice Hall*, 1992.

[2] M. Edwards, Y. Ni, M. Liang, A. Stammer, J. Massey, G. J. Vancso, and I. Manners. *Polymer Prepr., (Am. Chem. Soc. Div. Polym. Chem.)*, **34**:324, 1993.

[3] Y. Ni, A. Stammer, M. Liang, J. Massey, G. J. Vancso, and I. Manners. *Macromolecules*, **25**:7119, 1992.

[4] M. Liang and I. Manners. *J. Am. Chem. Soc.*, **113**:4044, 1991.

[5] H. N. Stokes. *Amer. Chem. J.*, **17**:275, 1895.

[6] H. N. Stokes. *Amer. Chem. J.*, **18**:629, 1896.

[7] H. N. Stokes. *Amer. Chem. J.*, **19**:782, 1897.

[8] K. H. Meyer, W. Lotmar, and G. W. Pankow. *Helv. Chim. Acta*, **19**:930, 1936.

[9] H. R. Allcock and R. L. Kugel. *J. Am. Chem. Soc.*, **87**:4216, 1965.

[10] H. R. Allcock, R. L. Kugel, and K. Valan. *J. Inorg. Chem.*, **5**:1709, 1966.

[11] H. R. Allcock and R. L. Kugel. *J. Inorg. Chem.*, **5**:1716, 1966.

[12] J. A. Dodge, I. Manners, G. Renner, H. R. Allcock, and O. J. Nuyken. *J. Am. Chem. Soc.*, **112**:1268, 1990.

[13] J. Jackle. *Rep. Prog. Phys.*, **49**:171, 1986.

[14] Pierre-Gilles de Gennes. *Scaling Concepts in Polymer Physics.* 1979. Cornell University Press, London.

[15] P.Hohenberg and W. Kohn. *Phys. Rev.*, **136**:B284, 1964.

[16] W. Kohn and L.J. Sham. *Phys. Rev.*, **140**:A1133, 1965.

[17] *deMon* is based on a program written by Alain St-Amant at the University of Montreal between 1988 and 1991 under the direction of Professor Dennis R. Salahub. The following list of principal contributing authors is complete as of June 1992: Alain St-Amant, Nathalie Godbout, Fiona Sim, The program is described in the following references: A. St-Amant, Ph. D. thesis, Universite de montreal, 1992; A. St-Amant and D. R. Salahub, *Chem. Phys. Lett.*, 1990 **169** 367; J. K. Labanowski and J. W. Andzelm, *Density Functional Methods in Chemistry*, (New York: Springer–Verlag) 1991.

[18] H. R. Allcock, R. W. Allen, and J. J. Meister. *Macromolecules*, **9**:950, 1976.

[19] W. J. Hehre, L. Radom, P. v.R. Schleyer, and J.A. Pople. *Ab Initio Molecular Orbital Theory.* John Wiley and Sons, Inc., New York, 1986.

[20] H. F. Schaefer, editor. *Modern Theoretical Chemistry: Applications of Electronic Structure Theory*, volume **4**. 1977. (Plenum Press, New York).

[21] J.B. Lagowski and G.J. Vancso. *Int. J. Quant. Chem.*, **46**:271, 1993.

[22] R. Jaeger, J.B. Lagowski, I. Manners, and G.J. Vancso. *Macromolecules,* (to be published), 1994.

[23] Graphical displays obtained using software programs, *Insight II*, from Biosym Technologies of San Diego.

[24] M. Levy and J. Perdew. *Density Functional Methods in Physics.* (Plenum, New York), 1985.

[25] W. Kohn and P. Vashishta. *Theory of the Inhomogeneous Electron Gas*, 1983.

[26] J. K. Labanowski and J. W. Andzelm. *Density Functional Methods in Chemistry.* Springer -Verlag, New York, 1991.

[27] R. G. Parr and W. Yang. *Density-Functional Theory of Atoms and Molecules.* (Oxford University, New York), 1989.

[28] D. R. Hartree. *Proc, Cambridge Phil. Soc.*, **24**:89, 1928.

[29] L. H. Thomas. *Proc, Cambridge Phil. Soc.*, **23**:542, 1927.

[30] E. Fermi. *Rend. Acad, Naz. Lincei*, **6**:602, 1927.

[31] S. H. Vosko, L. Wilk, and M. Nusair. *Can. J. Phys.*, **58**:1200, 1980.

[32] D. M. Ceperley and B. J. Alder. *Phys. Rev. Lett.*, **45**:566, 1980.

[33] L. Hedin and B. I. Lundqvist. *J. Phys. C: Solid State Phys.*, **4**:2064, 1971.

[34] R. Fournier, J. Andzelm, and D. R. Salahub. *J. Chem. Phys.*, **90**:6371, 1989.

[35] R. Fournier. *J. Chem. Phys.*, **92**:5422, 1990.

[36] B. I. Dunlap and J. Andzelm. *Phys. Rev. A*, **45**:81, 1992.

[37] P. Pulay. *Mol. Phys.*, **17**:197, 1969.

[38] P. Pulay. *Applications of Electronic Structure Theory.* H. F. Schaefer III, Ed., (Plenum, New York), 1977.

[39] S. M. Colwell, R. D¿ Amos, and N. C. Handy. *Chem. Phys. Lett.*, **109**:525, 1984.

[40] L. Fan, L. Versluis, T. Ziegler, E. J. Baerends, and W. Ravenek. *Int. J. Quant. Chem.*, **S22**:173, 1988.

[41] I. Papai, A. St-Amant, J. Ushio, and D. Salahub. *Int. J. Quant. Chem.*, **S24**:29, 1990.

[42] B. Schlegel. *Ab Initio Methods in Quantum Chemistry-I.* 1987. ed. K. P. Lawley, John Wiley and Sons Ltd., New York.

[43] Ed. S. Huzinaga. *Gaussian Basis Sets for Molecular Calculations.* (Elsevier, Amsterdam), 1984.

[44] H. Sambe and R. H. Felton. *J. Chem. Phys.*, **62**:1122, 1975.

[45] B. I. Dunlap, J. W. D. Connolly, and J. R. Sabin. *J. Chem. Phys.*, **71**:4993, 1979.

[46] S. Obara and A. Saika. *J. Chem. Phys.*,, **84**:3963, 1986.

[47] B. I. Dunlap. *J. Chem. Phys.*, **90**:5524, 1986.

[48] B. I. Dunlap and M. Cook. *Int. J. Quant. Chem.*, **29**:767, 1986.

[49] J. Andzelm, N.Russo, and D. R. Salahub. *J. Chem. Phys.*, **87**:6562, 1987.

[50] T. A. Koopmans. *Physica*, **1**:104, 1933.

[51] F. Herman and S. Skillman. *Atomic Structure Calculations, Prentice Hall, Englewood Cliffs.*, 1963.

[52] A. D. Becke. *J. Chem. Phys.*, **88**:2547, 1988a.

[53] V. I. Lebedev. *Zh. Vychisl. Mat. Mat. Fiz.*, **15**:48, 1975.

[54] V. I. Lebedev. *Zh. Vychisl. Mat. Mat. Fiz.*, **16**:293, 1976.

[55] A. V. Raja and J. B. Lagowski. *Int. J. Quant. Chem.*, (to be published), 1994.

[56] J.B. Lagowski, R. Jaeger, I. Manners, and G.J. Vancso. *Polymer Prepr., (Am. Chem. Soc. Div. Polym. Chem.)*, **34**:326, 1993.

[57] J. B. Lagowski and R. Jaeger. *Int. J. Quant. Chem.* (to be published), 1994.

[58] J.B. Lagowski, R. Jaeger, I. Manners, and G.J. Vancso. *Macromolecules* (to be published), 1994.

[59] M. J. S. Dewar, E. A. C. Lucken, and M. A. Whitehead. *J. Chem. Soc.*, page 2423, 1960.

[60] J. C. Slater. *Quantum Theory of Molecules and Solids*, volume **4**. McGraw Hill, New York, 1974.

[61] H. R. Allcock and F. W. Lampe. *Contemporary Polymer Chemistry*, volume **19**. 1990. 2nd ed.; Prentice Hall: Wnglewood Cliffs, NJ.

[62] P. J. Flory. *Statistical Mechanics of Chain Molecules*. 1969.

[63] J. B. Lagowski and G. J. Vancso. *Int. J. Quant. Chem.*, **46**:271, 1993.

[64] R. S. Mulliken. *J. Chem. Phys.*, **23**:1833, 1955.